Two-photon generation of excitonic molecules in CuCl: An exactly solvable bipolariton model and high-precision experiments

A.L. Ivanov
Institut für Theoretische Physik, J.W. Goethe Universität Frankfurt, Robert-Mayer-Strasse 8, D-60054 Frankfurt, Germany

M. Hasuo and N. Nagasawa
Department of Physics, School of Science, the University of Tokyo, 7-3-1 Hongo, Bunkyo-ku, Tokyo, Japan

H. Haug
Institut für Theoretische Physik, J.W. Goethe Universität Frankfurt, Robert-Mayer-Strasse 8, D-60054 Frankfurt, Germany
(Received 7 April 1995)

The conventional giant oscillator strength model of the two-photon (γ) generation of an excitonic molecule (m) attributes this process to the x-γ optical conversion (where x is the exciton), i.e., to the scheme $\gamma+\gamma\rightarrow x+\gamma\rightarrow m$. Recently [A.L. Ivanov and H. Haug, Phys. Rev. B **48**, 1490 (1993)], it was argued that a more adequate description can be done within the bipolariton model which follows the other scenario: $\gamma+\gamma\rightarrow x+x\rightarrow m$, where the Coulombic resonant coupling of the x components of the two interacting polaritons gives rise to the m formation. In the present work, we develop and analyze for the deuteron potential of an x-x interaction an exactly solvable bipolariton model of the two-γ m generation. This model treats an m optical creation in terms of the polariton-polariton resonant scattering and includes both the x-γ polariton coupling and the x-x attraction beyond a low-order perturbation theory. The bipolariton model and the giant oscillator strength model give different descriptions of the third-order m nonlinear optical susceptibility $\chi^{(3)}$ and of the two-γ m absorption. With the high-precision measurements in CuCl of the m radiative width Γ^m, $\chi^{(3)}$, and the two-γ m absorption coefficient $K^{(2)}$, we make a systematic comparison between the experiments and the two models, which allows us to unambiguously discriminate both models in favor of the bipolariton one.

I. INTRODUCTION

At low temperatures, excitonic molecules can be observed in luminescence of some direct band gap compound semiconductors of the groups I-VII and II-IV, e.g., CuCl, CuBr, CdS, etc. The m's can also be resonantly involved in various nonlinear optical processes such as two-photon absorption, hyper-Raman scattering, and four-wave mixing (for a review of biexciton optics see, e.g., Refs. 1 and 2). The high efficiency of these nonlinear processes has been attributed to (i) the virtual excitation of a transverse x with the energy ω_t, which is nearly resonant with half of the m total energy $\Omega^m/2$ and (ii) a giant oscillator strength of the $x\rightarrow m$ optical transition. The latter transition is described in terms of an optical conversion of the x into m,[3,4] i.e., $x+\gamma\rightarrow m$, where γ refers to a photon. Thus, the m optical creation, real or virtual, follows in this "giant oscillator strength model" the two-step elementary scheme:

$$\gamma(\mathbf{p})+\gamma(\mathbf{k})\longrightarrow x(\mathbf{p})+\gamma(\mathbf{k})\longrightarrow m(\mathbf{K}=\mathbf{p}+\mathbf{k})\,. \tag{1}$$

Here, $\mathbf{p}$, $\mathbf{k}$, and $\mathbf{K}$ are the crystal momenta ($\hbar=1$) of two incoming γ's and an m, respectively. Within the sequence of Eq. (1), one can either treat the $m(\mathbf{K}=\mathbf{p}+\mathbf{k})$ as a final product of two-γ absorption (regime of the real excitation) or continue further in a third step $m(\mathbf{K}=\mathbf{p}+\mathbf{k})\rightarrow x(\mathbf{p}_1)+\gamma(\mathbf{k}_1)$, which corresponds to hyper-Raman scattering, if the process is phase coherent, or to m luminescence, if the phase is lost.

An optical conversion $x+\gamma\rightarrow m$ is described in terms of the interaction $\frac{1}{\sqrt{V}}M_1(\mathbf{p},\mathbf{k})A^{\dagger}_{\mathbf{p}+\mathbf{k}}\alpha_{\mathbf{k}}B_{\mathbf{p}}$, where A, B, and α are the m, x, and γ operators, respectively, and V is the volume of a crystal. The matrix element $M_1(\mathbf{p},\mathbf{k})$ is given by

$$M_1(\mathbf{p},\mathbf{k})\;=\;-i\frac{\Omega_c}{2}\Psi_m\left(\frac{\mathbf{p}-\mathbf{k}}{2}\right)\,, \tag{2}$$

where $\Psi_m(\ell)$ is a Fourier transform of the internal m wave function, describing the relative motion of the two x's, Ω_c is the polariton parameter determined through a transverse-longitudinal splitting $\omega_{\ell t}$ by $\Omega_c=\sqrt{2\omega_{\ell t}\omega_t}$. The underlying physical picture of the $x\rightarrow m$ optical conversion is that in order to create an m one needs only to excite optically another x within spatial volume $\sim a_m^3$ around an already existing first x. Formally, a giant oscillator strength $f_m\sim\mid M_1\mid^2$ of this process is due to $\mid M_1(\mathbf{p},\mathbf{k})\mid^2\sim\mid\Psi_m\left(\frac{\mathbf{p}-\mathbf{k}}{2}\right)\mid^2\sim a_m^3\gg a_x^3$, where a_m and a_x are the m and x radii, respectively. The giant oscillator strength model and the concept of an optical conversion $x+\gamma\rightarrow m$ of Eqs. (1) and (2) are well accepted in biexciton physics both in theory[2,5–9] and for

the interpretation of experiments.[10–12,14–18]

However, more than 25 years ago Hopfield[19] recognized in the analysis of the giant oscillator strength of the linear absorption due to shallow x-impurity bound states that a self-consistent microscopic approach has to be formulated in terms of resonant polariton scattering at an x-impurity energy level. The cross section of the resonant Rayleigh polariton scattering has a spectral width Γ^i, where $1/\Gamma^i$ is attributed to the radiative lifetime of the x-impurity state. This conclusion is also a basic result of the general theory of resonant scattering at a quasidiscrete (metastable) level.[20]

The optical conversion to an m state resembles the linear absorption of the x-impurity bound state: in the transition $x + \gamma \rightarrow m$ the x plays role of an impurity, while the m corresponds to an x-impurity bound state. This analogy shows that one has to examine explicitly the polariton-polariton resonant scattering due to a metastable m state in a first-principles treatment of the two-γ m generation. This fact has been recognized in our previous work[21] where we proposed the following scenario of the m two-γ creation:

$$\gamma(\mathbf{p}) + \gamma(\mathbf{k}) \longrightarrow x(\mathbf{p}) + x(\mathbf{k}) \longrightarrow m(\mathbf{K} = \mathbf{p} + \mathbf{k}) \,. \tag{3}$$

In further analysis we will refer to Eq. (3) as a "bipolariton model." The second step of Eq. (3) is determined by the Coulombic interaction $\frac{1}{\sqrt{V}} M_2(\mathbf{p},\mathbf{k}) A^{\dagger}_{\mathbf{p}+\mathbf{k}} B_{\mathbf{p}} B_{\mathbf{k}}$ and corresponds to the polariton-polariton scattering due to interaction of their x components. Within this picture, the matrix element $M_2(\mathbf{p},\mathbf{k})$ has been derived:[21]

$$M_2(\mathbf{p},\mathbf{k}) = -\left[\epsilon^m + \frac{(\mathbf{p}-\mathbf{k})^2}{4M_x}\right] \Psi_m\left(\frac{\mathbf{p}-\mathbf{k}}{2}\right) , \tag{4}$$

where ϵ^m is the m binding energy, M_x is the x translational mass.

The polariton dispersion allows one to satisfy the energy-momentum conservation in the scattering $x + x \rightarrow m$ (see Fig. 1). In other words, the virtually excited x's with the polariton energies $\omega_p = \omega^{\mathrm{pol}}(p)$ and $\omega_k = \omega^{\mathrm{pol}}(k)$ couple resonantly to the m state. This virtual optical excitation process is very efficient because the polariton parameter $\Omega_c \gg \epsilon^m$. For CuCl, e.g., one has $\Omega_c \simeq 191$ meV and $\epsilon^m \simeq 34$ meV. Without the polariton effect, a resonant m generation by two x's is not possible. On the contrary, for the inverse process of the radiative decay, an m state has to be treated within the polariton picture as a quasibound "bipolariton."[22] Thus, our approach replaces the concept of a biexciton by that of a bipolariton.

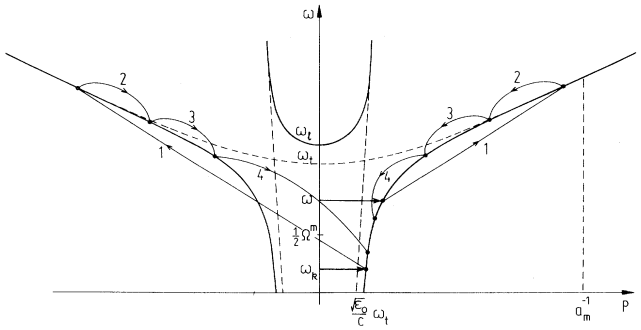

FIG. 1. Schematic picture of the resonant polariton-polariton scattering due to an m. The first (1), the following (2 and 3), and the last (4) elementary Coulombic scattering acts are indicated.

The giant oscillator strength scheme of Eq. (1) masks completely x-x (polariton-polariton) scattering, which causes a change of the initial γ momenta $\mathbf{p}$ and $\mathbf{k}$ and gives rise to m creation. The second step of this model, i.e., the optical conversion $x + \gamma \rightarrow m$, implies that the second x that is optically created within an m volume a_m^3 around the first x *always* undergoes scattering. In the general case this statement is not true because both processes, the $x \leftrightarrow \gamma$ polariton coupling and the $x + x \rightarrow m$ Coulombic scattering, are resonant. For a correct description of the m optical properties one has to examine the scheme of Eq. (3) beyond a perturbational treatment of the polariton and Coulombic interactions. In the second step of this bipolariton model one recovers an important feature of the giant oscillator strength model. Due to the spatially extended m wave function $\Psi_m\left(\frac{\mathbf{p}-\mathbf{k}}{2}\right)$ in the matrix element $M_2(\mathbf{p},\mathbf{k})$ of Eq. (4), the x with momentum $\mathbf{k}$ acts again like an "antenna" that collects the second x with momentum $\mathbf{p}$ from the whole coherent m volume, because the cross section of resonant x-x scattering is proportional to $|\, M_2(\mathbf{p},\mathbf{k})\,|^2 \sim a_m^3$.

In the polariton representation, both schemes reduce to a single one: $\gamma + \gamma \rightarrow$ polariton + polariton $\rightarrow m$, however, with different basic interactions. As a result, the two models lead to measurable differences in the description of the x-m optical Stark effect, hyper-Raman scattering, m luminescence, and even two-γ (two-polariton) m absorption.

In spite of the considerable success of the giant oscillator strength model for m's in bulk semiconductors, novel high precision techniques[14–18] with a spectral resolution ≤ 10 μeV at the lowest pump intensities ~ 1 kW/cm^2 allow one to investigate experimentally detailed features of the m nonlinear optical properties and discriminate between both models. CuCl is the best candidate for such experiments due to anomalously weak x-LA-phonon interaction.[1,23] At low temperatures $T \leq 10$ K, an m with the given momentum $\mathbf{K}$ mainly decays radiatively in CuCl before it is scattered by LA phonons.[15] Thus, one can treat an $x - \gamma - m$ system as a conservative, closed dynamical system and without introducing any phenomenological damping constant for the m state.

In Ref. 21 we proposed and analyzed the bipolariton scheme of Eq. (3). However, although the x-x scattering has been included as the mechanism responsible for the m optical generation, the complete scattering model with a nonperturbative treatment of both x-γ and x-x interactions has not been developed. In our approach, the wave fuction $\Psi_m\left(\frac{\mathbf{p}-\mathbf{k}}{2}\right) = \Psi_0\left(\frac{\mathbf{p}-\mathbf{k}}{2}\right)$ in the matrix elements $M_1(\mathbf{p},\mathbf{k})$ and $M_2(\mathbf{p},\mathbf{k})$ has been treated within a standard biexciton Schrödinger equation, which yields a

stable m ground state without the influence of the polariton effects. However, the true concept of a bipolariton includes both x-γ and x-x couplings from the very beginning and results in a metastable m state.[22] Instead of a wave function Ψ_0, which is unperturbed by the polariton effects, one has to deal with the exact one, $\tilde{\Psi}$, which describes two outgoing polariton waves as a result of the optical decay and corresponds to the true bipolariton state.

In this paper, we (i) develop an exactly solvable microscopic bipolariton model within the scenario of Eq. (3) and (ii) report experimental evidence in support of this scheme.

In Sec. II the bipolariton model is developed on the basis of the microscopic x-γ Hamiltonian. In order to describe the two-γ m generation in terms of polariton-polariton resonant scattering we use Belyaev's diagram technique. Then, the problem reduces to the analysis of a homogeneous Bethe-Salpeter equation for the m vertex function which includes both the x-x and x-γ interactions. The exactly solvable bipolariton model is developed for a deuteron model potential of the x-x attraction. The total resonant nonlinear susceptibility associated with an m is found. In the low-excitation limit, the m radiative width Γ^m, the third-order m nonlinear susceptibility $\chi^{(3)}$, and the two-γ m absorption coefficient $K^{(2)}$ are calculated within the bipolariton model.

In Sec. III we summarize the m optical properties of the giant oscillator strength model which deals with the semiphenomenological x-γ-m Hamiltonian.

In Sec. IV the descriptions and results of the high-precision measurements of Γ^m, $\chi^{(3)}$, and $K^{(2)}$ in CuCl are given. From the comparison between the experiments and the two models we conclude the advantages of the bipolariton model over the giant oscillator strength one.

II. EXACTLY SOLVABLE BIPOLARITON MODEL FOR BIEXCITON OPTICAL GENERATION

In this section we develop the bipolariton model for the self-consistent description of the optical nonlinearities due to the excitonic molecules.

A. Model

In this subsection we discuss the adiabatic approximation that allows us to reduce the initial electron-hole-photon (e-h-γ) picture to the x-γ one. Then, we adopt Belyaev's diagram technique to calculate the total resonant m nonlinear susceptibility χ within the bipolariton model and show how one can extract from the total χ the third-order optical nonlinear susceptibility $\chi^{(3)}$.

For a description of the optical properties of a semiconductor (e.g., CuCl) near an x ground-state resonance, the initial e-h-γ Hamiltonian can be reduced to the x-γ representation[21,24] ($\hbar = 1$):

$$H = \sum_{\sigma,\mathbf{p}} \Big[\omega^x(p) B^\dagger_{\sigma\mathbf{p}} B_{\sigma\mathbf{p}} + \omega^\gamma(p) \alpha^\dagger_{\sigma\mathbf{p}} \alpha_{\sigma\mathbf{p}} + \frac{i\Omega_c}{2} \left(\alpha^\dagger_{\sigma\mathbf{p}} B_{\sigma\mathbf{p}} - B^\dagger_{\sigma\mathbf{p}} \alpha_{\sigma\mathbf{p}} \right) + \sum_{\sigma',l,\mathbf{q}} W_{\sigma\sigma'}(q) B^\dagger_{\sigma\mathbf{p}} B^\dagger_{\sigma' l} B_{\sigma' l+\mathbf{q}} B_{\sigma\mathbf{p}-\mathbf{q}} \Big] , \quad (5)$$

where $\omega^x(p) = \omega_t + p^2/2M_x$ and $\omega^\gamma(p) = cp/\sqrt{\varepsilon_0}$ are the x and γ dispersions, respectively, ε_0 is the background optical dielectric constant. The symbol $\sigma = 1, 2$ refers to the two possible circular polarizations (clockwise σ^+ or counterclockwise σ^-) of light which resonate with the x level. The corresponding dipole-active x's with $\sigma = 1$ and

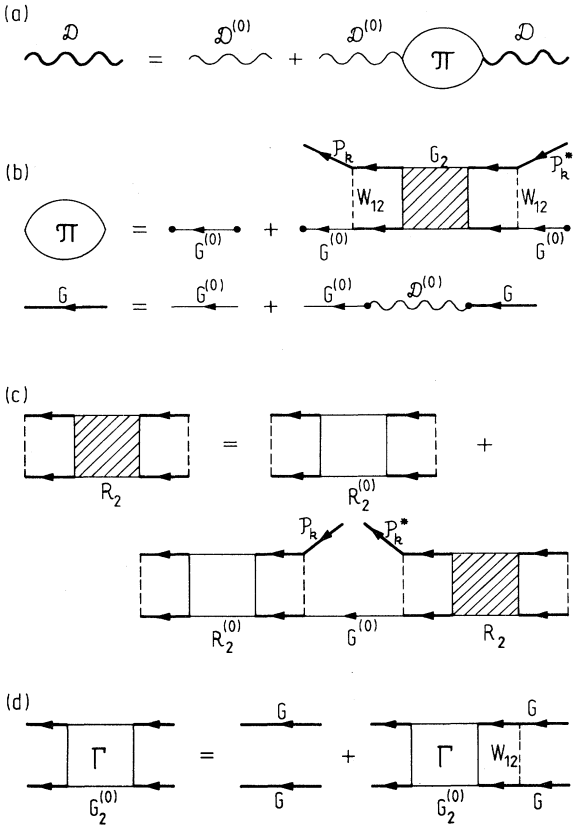

FIG. 2. Diagram equations for the polariton-polariton resonant scattering. D and $D^{(0)}$ are the complete and free-particle retarded γ Green functions, respectively; Π is the polarization operator; G_2 and $G_2^{(0)}$ are the two-x Green functions, renormalized and unperturbed by the pump wave, respectively; R_2 and $R_2^{(0)}$ are the integral convolutions given by Eq. (12) of the potential W_{12} with G_2 and $G_2^{(0)}$, respectively; $\mathcal{P}_\mathbf{k}$ is the amplitude of coherent x polarization of the pump. A bold dot symbolizes the x-γ polariton coupling, a dashed line corresponds to the x-x Coulombic attraction potential W_{12}. (a) Dyson equation for the γ field of the probe. (b) Equation for the polarization operator Π of the probe light and the polariton equation for the x Green function G. (c) Equation for the two-x function R_2 renormalized by the pump. (d) Bethe-Salpeter equation for $G_2^{(0)}$. This equation includes both the x-γ polariton coupling and the x-x interaction.

2 have different spin structures: $e\uparrow, h\downarrow$ for $\sigma = 1$, and $e\downarrow, h\uparrow$ for $\sigma = 2$. The potentials $W_{\sigma\sigma'}$ of the x-x interactions can be given explicitly[24] as integral convolutions of the various pair $e(h)$-$e(h)$ Coulomb potentials with the x wave functions. Due to exchange interaction, $W_{11}(q)$, $W_{22}(q) > 0$, i.e., x's with the same spin structure always repel each other, while $W_{12}(q) = W_{21}(q) < 0$. This attractive potential is responsible for an m formation with the spin structure $e\uparrow, e\downarrow, h\uparrow, h\downarrow$.

The x-γ picture of Eq. (5) is correct in the low-density limit $Na_x^3 \ll 1$.[21,24] Here, N is the concentration of x's excited really or virtually by light. This limit holds in usual m optics, where one needs considerably weaker excitations $Na_m^3 \leq 1$. Furthermore, Eqs. (2), (4), and (5) are appropriate for an m description in the adiabatic approximation, when the x binding energy $\epsilon^x \gg \epsilon^m$. This approximation is valid for CuCl: $\epsilon^x \simeq 190$ meV and $\epsilon^m \simeq 34$ meV. In the adiabatic approximation an m is treated as a bound state of the two x's with different spin structures; the corresponding m operator $A_{\mathbf{K}}$ is given by

$$A_{\mathbf{K}} = \frac{1}{\sqrt{V}} \sum_{l} \Psi_m(l) B_{1,l+\mathbf{K}/2} B_{2,-l+\mathbf{K}/2} \cdot \quad (6)$$

The x-γ Hamiltonian of Eq. (5) treats the x's as structureless quasiparticles and includes both basic interactions: the x-γ polariton coupling and the x-x Coulombic interactions. Then, an m introduced by Eq. (6) can be analyzed within Eq. (5). Recently, this model with the two spin states for x's and the corresponding two polarizations for γ's has been adopted for intermediate excitations, $Na_m^3 \geq 1 \geq Na_x^3$, with simplified contact potentials $W_{11}(q) = W_{22}(q) = U = \text{const} > 0$ and $W_{12}(q) = W_{21}(q) = W = \text{const} < 0$.[25]

We consider a coherent polariton pump wave $\mathbf{k}$, $\omega_{\mathbf{k}}$ ($\sigma = 2$) and a polariton probe wave $\mathbf{p}$, ω ($\sigma = 1$) with the intensities $I_{\mathbf{k}} \gg I_0$. The two polariton waves are nearly resonant with the m: $\omega + \omega_{\mathbf{k}} \simeq \widetilde{\Omega}^m_{\mathbf{p}+\mathbf{k}}$ (see Fig. 1), where $\widetilde{\Omega}^m_K$ is the m energy. We use the Hamiltonian of Eq. (5) given in the x-γ representation rather than its polariton representation. This allows one to see explicitly the influence of the both basic interactions, x-γ and x-x, on the m optical properties. For the coherent pump we use Belyaev's diagram technique (see, e.g., Ref. 26).

The probe wave is described by the complete single-particle γ Green function D, which is determined by the following equation [see Fig. 2(a)]:

$$D = D^{(0)} + D^{(0)} \Pi D \,, \quad (7)$$

where $D^{(0)}(\mathbf{p},\omega) = 1/[\omega^2 - \omega^\gamma(p)^2]$ is the free-particle γ propagator and Π is the polarization operator. The optical susceptibility χ of the probe field is given in terms of the polarization operator by

$$\chi = \chi(\mathbf{p},\omega;\mathbf{k},\omega_{\mathbf{k}},I_{\mathbf{k}}) = -\frac{\varepsilon_0}{2\pi\omega^2}\omega_t \Pi(\mathbf{p},\omega;\mathbf{k},\omega_{\mathbf{k}},I_{\mathbf{k}}). \quad (8)$$

In accordance with the diagrams of Fig. 2(b), a resonant part of the polarization operator Π is determined by an x and an m component:

$$\Pi(\mathbf{p},\omega;\mathbf{k},\omega_{\mathbf{k}},I_{\mathbf{k}}) = \Pi_x(\mathbf{p},\omega) + \Pi_m(\mathbf{p},\omega;\mathbf{k},\omega_{\mathbf{k}},I_{\mathbf{k}}) \,, \quad (9)$$

where

$$\Pi_x(\mathbf{p},\omega) = \tfrac{1}{4}\,\Omega_c^2\, G^{(0)}(\mathbf{p},\omega) \,, \quad (10)$$

$$\Pi_m(\mathbf{p},\omega;\mathbf{k},\omega_{\mathbf{k}},I_{\mathbf{k}}) = \tfrac{1}{4}\,\Omega_c^2 G^{(0)}(\mathbf{p},\omega) \mid \mathcal{P}_{\mathbf{k}} \mid^2 \times R_2(\mathbf{p},\omega;\mathbf{k},\omega_{\mathbf{k}},I_{\mathbf{k}}) G^{(0)}(\mathbf{p},\omega) \,. \quad (11)$$

Here, $G^{(0)}(\mathbf{p},\omega) = 1/[\omega - \omega^x(p) + i\delta]$ is the free-particle x Green function, $\mid \mathcal{P}_{\mathbf{k}} \mid^2 = \frac{1}{V}\langle B_{\mathbf{k}}\rangle \langle B^\dagger_{\mathbf{k}}\rangle \sim I_{\mathbf{k}}$ is the transient concentration of coherent x's virtually excited by a pump (x component of the polariton pump), and the function R_2 is given by

$$R_2(\mathbf{p},\omega;\mathbf{k},\omega_{\mathbf{k}},I_{\mathbf{k}}) = \sum_{\mathbf{q}_1,\mathbf{q}_2} \int d\omega_1 d\omega_2 \; W_{12}(q_1) W_{12}(q_2) \times G_2(\mathbf{k}+\mathbf{q}_1, \omega_{\mathbf{k}}+\omega_1; \mathbf{p}-\mathbf{q}_1, \omega-\omega_1; \mathbf{k}+\mathbf{q}_2, \omega_{\mathbf{k}}+\omega_2; \mathbf{k}-\mathbf{q}_2, \omega-\omega_2; I_{\mathbf{k}}) \,, \quad (12)$$

where G_2 is the two-x Green function renormalized by the pump-probe resonant Coulombic interaction. The corresponding diagram equation for the function R_2 shown in Fig. 2(c) reduces to

$$R_2(\mathbf{p},\omega;\mathbf{k},\omega_{\mathbf{k}},I_{\mathbf{k}}) = R_2^{(0)}(\mathbf{p},\omega;\mathbf{k},\omega_{\mathbf{k}}) + R_2^{(0)}(\mathbf{p},\omega;\mathbf{k},\omega_{\mathbf{k}}) \mid \mathcal{P}_{\mathbf{k}} \mid^2 G^{(0)}(\mathbf{p},\omega) R_2(\mathbf{p},\omega;\mathbf{k},\omega_{\mathbf{k}},I_{\mathbf{k}}) \,, \quad (13)$$

where $R_2^{(0)}$ is given by Eq. (12) with G_2 replaced on $G_2^{(0)}$—the two-x propagator unperturbed by the coherent pump. In accordance with Fig. 2(c), the diagrams of Eq. (13) do not contain explicitly any wavy lines [γ Green functions $D^{(0)}(\mathbf{p},\omega)$] between different $G_2^{(0)}$, because the polarization operator Π_m is irreducible with respect to the x-γ coupling of the probe.

A nonresonant part $\Pi^{\text{nr}}_{x\text{-}x}$ of the polarization operator Π is given by the graph of Fig. 3(a) for a normal contribution (one absorbed and one emitted pump γ) and by the graphs of Fig. 3(b) for an anomalous contribution (two absorbed pump γ's, etc.). All these graphs do not contain the m pole. For the anomalous graphs (in Belyaev's technique notations) of Fig. 3(b) this conclusion is due to the optical selection rules: the two pump γ's of the given circular polarization do not excite an m. As a result, a contribution of $\Pi^{\text{nr}}_{x\text{-}x}$ to the m optical response is rather small in comparison with Π_m of Eq. (9). Formally, $\Pi_m \sim a_m^3/(\widetilde{\Omega}^m_{\mathbf{p}+\mathbf{k}} - \omega - \omega_{\mathbf{k}})$, while the large m volume factor a_m^3 and the m resonant denominator are absent in $\Pi^{\text{nr}}_{x\text{-}x}$.

The total optical susceptibility χ of Eq. (8) can be

presented in the following form:

$$\chi(\mathbf{p},\omega;\mathbf{k},\omega_{\mathbf{k}},I_{\mathbf{k}}) = \chi_0(\mathbf{p},\omega) + \chi_{\rm nl}^{\rm odd}(\mathbf{p},\omega;\mathbf{k},\omega_{\mathbf{k}},I_{\mathbf{k}}) , \tag{14}$$

where χ_0 is the standard linear x susceptibility and $\chi_{\rm nl}^{\rm odd}$ is the total nonlinear susceptibility induced by the coherent pump. Together with the eigenmode relationship $p^2c^2 = \varepsilon(\mathbf{p},\omega)\omega^2$, the linear part χ_0, which is given by the first component $\Pi_x(\omega,\mathbf{p})$ of the polarization operator Π, yields the probe polariton spectrum unperturbed by a pump. The nonlinear part $\chi_{\rm nl}^{\rm odd}$ due to the second component $\Pi_m(\mathbf{p},\omega;\mathbf{k},\omega_{\mathbf{k}},I_{\mathbf{k}})$ of Π includes a whole set of the odd-order susceptibilites:

$$\chi_{\rm nl}^{\rm odd}(\mathbf{p},\omega;\mathbf{k},\omega_{\mathbf{k}},I_{\mathbf{k}}) = \chi^{(3)}(\omega=\omega_{\mathbf{k}}-\omega_{\mathbf{k}}+\omega;\omega_{\mathbf{k}},-\omega_{\mathbf{k}},\omega) + \sum_{n=2}^{\infty}\chi^{(2n+1)}(\mathbf{p},\omega;\mathbf{k},\omega_{\mathbf{k}})I_{\mathbf{k}}^{n-1} . \tag{15}$$

From Eqs. (9)–(13) one gets

$$\Pi(\mathbf{p},\omega;\mathbf{k},\omega_{\mathbf{k}},I_{\mathbf{k}}) = \frac{\Omega_c^2 G^{(0)}(\mathbf{p},\omega)}{1 - G^{(0)}(\mathbf{p},\omega)\mid P_{\mathbf{k}}\mid^2 R_2^{(0)}(\mathbf{p},\omega;\mathbf{k},\omega_{\mathbf{k}})} , \tag{16}$$

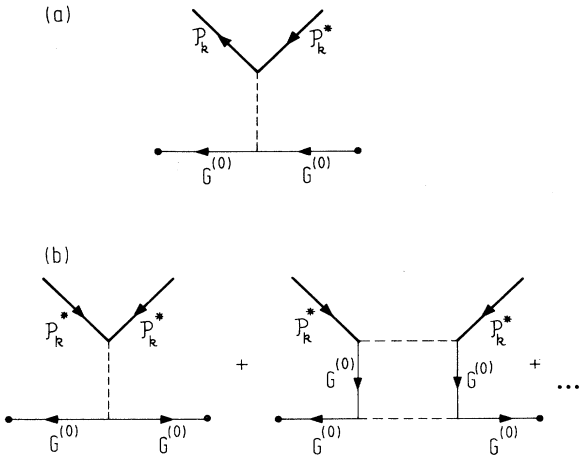

FIG. 3. Diagrams of the normal (a) and anomalous (b) contributions to the nonresonant part $\Pi_{x\to x}^{\rm nr}$ of the m polarization operator Π.

In order to calculate Π one needs the m function $R_2^{(0)}(\mathbf{p},\omega;\mathbf{k},\omega_{\mathbf{k}})$. The equation for the m propagator $G_2^{(0)}$ is given by the Bethe-Salpeter equation of Fig. 2(d). This two-x Green function $G_2^{(0)}$ can be expanded into the eigenfunctions $\widetilde{\Psi}^{(n)}$ of the relative motion of the two x's ($n = 0, ..., \infty$, i.e., disctrete and continuous spectrum):

$$\int d\omega_1 d\omega_2 G_2^{(0)}(\mathbf{k}+\mathbf{q}_1,\omega_{\mathbf{k}}+\omega_1;\mathbf{p}-\mathbf{q}_1,\omega-\omega_1;\mathbf{k}+\mathbf{q}_2,\omega_{\mathbf{k}}+\omega_2;\mathbf{k}-\mathbf{q}_2,\omega-\omega_2) = \sum_n \frac{\widetilde{\Psi}^{(n)}(\frac{\mathbf{p}-\mathbf{k}}{2}-\mathbf{q}_1)\widetilde{\Psi}^{(n)*}(\frac{\mathbf{p}-\mathbf{k}}{2}-\mathbf{q}_2)}{\omega+\omega_{\mathbf{k}}-\widetilde{\Omega}_{\mathbf{p}+\mathbf{k}}^{m(n)}+i\delta} . \tag{17}$$

Equation (17) is a general property of the two-particle Green functions.[27] In the spectral vicinity of the lowest m resonance ($n = 0$) $R_2^{(0)}$ reduces with Eqs. (12) and (17) to

$$R_2^{(0)}(\mathbf{p},\omega;\mathbf{k},\omega_{\mathbf{k}})) = \sum_{\mathbf{q}_1,\mathbf{q}_2} W_{12}(q_1)W_{12}(q_2)\frac{\widetilde{\Psi}(\frac{\mathbf{p}-\mathbf{k}}{2}-\mathbf{q}_1)\widetilde{\Psi}^*(\frac{\mathbf{p}-\mathbf{k}}{2}-\mathbf{q}_2)}{\omega+\omega_{\mathbf{k}}-\widetilde{\Omega}_{\mathbf{p}+\mathbf{k}}^{m}+i\delta} , \tag{18}$$

where $\widetilde{\Omega}_{\mathbf{K}=\mathbf{p}+\mathbf{k}}^{m} = \widetilde{\Omega}_{\mathbf{K}=\mathbf{p}+\mathbf{k}}^{m(n=0)}$. The final solution of Eqs. (8) and (16) with Eq. (18) depends on the m ground-state wave function $\widetilde{\Psi}$ with the energy $\widetilde{\Omega}^m$. These functions have to be determined from the corresponding m Schrödinger equation.

In the giant oscillator strength model, one separates the x-γ polariton coupling from the x-x Coulombic interaction. In this approach, at first the m ground state and energy are calculated variationally within the underlying e-h picture.[28] In the x representation the corresponding m Schrödinger equation is

$$\left[\omega^x\left(l+\frac{\mathbf{K}}{2}\right)+\omega^x\left(-l+\frac{\mathbf{K}}{2}\right)\right]\Psi_0(l,\mathbf{K}) + \sum_{l'} W_{12}(l-l')\Psi_0(l',\mathbf{K}) = \Omega_K^{m(0)}\Psi_0(l,\mathbf{K}) . \tag{19}$$

Due to the quadratic x dispersion the center-of-mass motion splits off in Eq. (19), i.e., $\Psi_0(l,\mathbf{K}') = \delta(\mathbf{K}-\mathbf{K}')\Psi_0(\ell)$. The wave function $\Psi_0(\ell)$ of the relative motion and the corresponding m binding energy $-\epsilon_0^m = \Omega_K^{m(0)} - K^2/2M_m - 2\omega_t < 0$ are real and independent of $\mathbf{K}$. Here, $M_m = 2M_x$ is the m translational mass. As a second step of this scheme, the m optical properties are attributed to the $m \leftrightarrow x+\gamma$ optical conversion with the matrix element of Eq. (2) which follows the m wave function $\Psi_m = \Psi_0$ and $\widetilde{\Omega}^m = \Omega^{m(0)}$.

In the analysis[21] of the scenario of Eq. (3) with the matrix element $M_2(\mathbf{p},\mathbf{k})$ given by Eq. (4) we have also

assumed $\Psi_m = \Psi_0$ and $\epsilon^m = \epsilon_0^m$. Such an introduction of both matrix elements $M_1(\mathbf{p},\mathbf{k})$ and $M_2(\mathbf{p},\mathbf{k})$ with $\Psi_m = \Psi_0$ considerably simplifies the theoretical models of Eqs. (1) and (3), respectively. Moreover, this assumption, which treats an m within Eq. (19) as a stable quasiparticle, cannot allow us to construct a correct theory of x-x (polariton-polariton) resonant scattering. In order to develop this theory one has to treat an m as a *metastable* "ground state" of the two quasibound polaritons. Thus, the self-consistent m Schrödinger equation has to include both basic x-γ and x-x interactions.

In conclusion, we found in this subsection the general expression for the total χ associated with an m ground state. This expression includes the m wave function $\widetilde{\Psi}$, which is still unknown and should be found self-consistently within the bipolariton model.

B. Bipolariton wave equation

In this subsection, a Schrödinger equation for an excitonic molecule is derived within the bipolariton model. This bipolariton wave equation contains both the x-x Coulombic attraction and the x-γ polariton coupling. It is solved for the deuteron model potential of the x-x attraction. The solution describes an m as a quasibound two-polariton complex. The real and imaginary parts of the m energy give the radiative renormalization Δ^m of the m energy (the m Lamb shift) and the inverse m radiative lifetime Γ^m, respectively. Then, the exact bipolariton wave function $\widetilde{\Psi}$ allows us to find self-consistently within the bipolariton model the total m nonlinear susceptibility χ.

The wave equation (19) can be obtained from the corresponding *homogeneous* Bethe-Salpeter equation[27] for the x-x vertex function $\Gamma_0(l,l';K)$ unperturbed by the polariton effects. Here, $l = (\boldsymbol{l},\omega)$ and $l' = (\boldsymbol{l}',\omega')$ are the reduced relative momenta and frequencies of two x's before and after the interaction act; $K = (\mathbf{K},\Omega)$ is the conserved total momentum and energy. In the diagram representation of Fig. 2(d), this equation ascribes the internal solid lines to the free x Green function $G^{(0)}$. However, the diagrams of Figs. 2(b) and 2(d) show that the polariton effect can be included self-consistently if one attributes the internal solid lines to the x-polariton Green function $G = G^{(0)} + \frac{1}{2}\Omega_c^2 G^{(0)} D^{(0)} G$ (bold solid line). Then, the homogeneous Bethe-Salpeter equation of Fig. 2(d) reduces to the following bipolariton wave equation:

$$\left[\omega^{\rm pol}\left(\boldsymbol{l}+\frac{\mathbf{K}}{2}\right)+\omega^{\rm pol}\left(-\boldsymbol{l}+\frac{\mathbf{K}}{2}\right)\right]\widetilde{\Psi}(l,\mathbf{K}) + \sum_{l'}\widetilde{W}_{12}(l,l',\mathbf{K})\widetilde{\Psi}(l',\mathbf{K}) = \widetilde{\Omega}_K^m\widetilde{\Psi}(l,\mathbf{K}) \quad (20)$$

with $\omega^{\rm pol}(\mathbf{p}) = \omega^-(p)$. Here, $\omega^\pm(p)$ are the dispersions of the upper (+) and lower (−) polariton branches, respectively, i.e., the roots of the polariton dispersion equation:

$$\omega^\gamma(p)^2 = \frac{c^2p^2}{\varepsilon_0} = \omega^2 + \frac{\Omega_c^2\omega^2}{\omega_t^2+\omega_t p^2/M_x-\omega^2}\,. \quad (21)$$

The effective potential $\widetilde{W}_{12}$ is determined by the x components of the two interacting polaritons:

$$\widetilde{W}_{12}(\boldsymbol{l},\boldsymbol{l}',\mathbf{K}) = f(\boldsymbol{l},\mathbf{K})W_{12}(\boldsymbol{l}-\boldsymbol{l}')\,, \quad (22)$$

where

$$f(\boldsymbol{l},\mathbf{K}) = \varphi^-(\boldsymbol{l}+\mathbf{K}/2,\omega^-(\boldsymbol{l}+\mathbf{K}/2)) \times\varphi^-(-\boldsymbol{l}+\mathbf{K}/2,\omega^-(-\boldsymbol{l}+\mathbf{K}/2)) \quad (23)$$

and

$$\varphi^\pm(\mathbf{p},\omega) = \frac{\omega^\pm(\mathbf{p})\,[\omega-\omega^\gamma(\mathbf{p})]}{\omega\,[\omega^\pm(\mathbf{p})-\omega^\mp(\mathbf{p})]}\,. \quad (24)$$

The x weight functions $\varphi^\pm(\mathbf{p},\omega)$ satisfy the conditions

$$\varphi^+(\mathbf{p},\omega^+(\mathbf{p})) \geq 0\,, \quad \varphi^-(\mathbf{p},\omega^-(\mathbf{p})) \geq 0\,, \quad \varphi^+(\mathbf{p},\omega^+(\mathbf{p})) + \varphi^-(\mathbf{p},\omega^-(\mathbf{p})) = 1\,. \quad (25)$$

These functions describe the x components in the two branches ($\pm$) of the polariton dispersion. The last relation is a "sum rule" of the x-γ polariton transition. Although the m wave equation with the polariton effects can be derived in a general form which includes both the upper and lower polariton branches, in Eq. (20) we restrict ourselves to the lower branch. This approximation holds because the lower polariton branch changes continuously into the x dispersion for $p > k_{\rm opt} = \omega_t\sqrt{\varepsilon_0}/c$, and because the density of states of the lower polariton branch exceeds considerably that of the upper one.

According to Eq. (20) the Coulombic longitudinal x-x interaction cannot be separated from the x-γ coupling. Here, we have a unique example where both the Coulombic x-x interaction and the polariton coupling can be treated exactly within the adiabatic approximation. This equation shows that the true components of an m are the two polaritons quasibound through the Coulombic interaction, rather than the two x's. Actually the word "bipolariton" is more adequate than "biexciton." The importance of the bipolariton concept has been recognized already in Refs. 13 and 29.

An exactly solvable bipolariton model for the m optical nonlinearities exists, provided one knows the analytical solution of the bipolariton Schrödinger equation (20). The quasistationary solution $\widetilde{\Psi}(\mathbf{p},\mathbf{K})$ with $\widetilde{\Omega}_K^m$ of Eq. (20) has to satisfy the appropriate boundary condition: the wave function $\widetilde{\Psi}$ in real space has to represent an outgoing spherical polariton wave at infinity. The identical boundary condition takes place for the resonant polariton-polariton scattering. This allows us to use the solution of the bipolariton wave equation (20) (or the corresponding homogeneous Bethe-Salpeter equation) in the resonant polariton-polariton scattering. In this approach, the equation for the two-x Green function $G_2^{(0)}$ shown in Fig. 2(d) summarizes for the two interacting polaritons a whole ladder set of the elementary Coulombic interactions. The first act of resonant scattering throws with a high probability the initial po-

laritons with p, $k \sim k_{\rm opt}$ to the x-like part of the lower polariton branch. The corresponding momenta are p', $k' \sim 1/a_m$. Then the two scattered x's evolve due to the x-x Coulombic interaction acts inside the m basic region $\sim 1/a_m$ in momentum space, an m exists as a transient metastable state without strong coupling with γ's (see Fig. 1). Finally, at a last scattering act, at least one of the two interacting x's reaches again the region of small momenta from the optical range and converts into an outgoing polariton. Thus, an m optical decay or complete polariton-polariton scattering occurs. According to a general theorem of the scattering theory,[26] the m vertex function $\Gamma(l,l';K)$ determines straightforwardly an x-x (polariton-polariton) scattering amplitude. In order to adopt these variables to Eq. (18) one has to put $\boldsymbol{l} = (\mathbf{p}-\mathbf{k})/2$ and $\mathbf{K} = \mathbf{p}+\mathbf{k}$.

The complex boundary condition (outgoing wave at infinity) gives for Eq. (20) a complex value of the bipolariton energy $\widetilde{\Omega}_K^m = \Omega_K^{m(0)} + \Delta^m(K) - i\widetilde{\Gamma}^m(K)/2$. Here, $\Omega_K^{m(0)} = \Omega_{K=0}^{m(0)} + K^2/2M_m$ is the m energy of Eq. (19) unperturbed by the polariton effects, $\widetilde{\Gamma}^m$ is the inverse m radiative lifetime, and Δ^m is the radiative renormalization of the m energy (the m Lamb shift), respectively.

In Ref. 22 we have found an analytical solution of the bipolariton equation (20) for a model potential W_{12} of the x-x attraction. Namely, for the deuteron potential

$$W_{12}(\boldsymbol{l}-\boldsymbol{l}') = \frac{W_{12}(0)}{[(\boldsymbol{l}-\boldsymbol{l}')^2+1]^2} \tag{26}$$

with $W_{12}(0) = -54\pi$, the solution of Eq. (20) is given by

$$\widetilde{\Psi}(\boldsymbol{l},\mathbf{K}) = -\frac{f(\boldsymbol{l},\mathbf{K})}{\delta\widetilde{\Omega}(\boldsymbol{l},\mathbf{K})}\left[(l^2/M_x+\epsilon_0^m)\Psi_0(l) + \frac{W_{12}(l)C}{(2\pi)^3}\right], \tag{27}$$

$$\widetilde{\Omega}_K^m - \Omega_K^{m(0)} = \Delta^m(K) - i\widetilde{\Gamma}^m(K)/2 = -\frac{27}{32\pi^{5/2}}C(\widetilde{\Omega}_K^m), \tag{28}$$

where

$$\delta\widetilde{\Omega}(\boldsymbol{l},\mathbf{K}) = \widetilde{\Omega}_{\mathbf{K}}^m - \omega^-\left(\boldsymbol{l}+\frac{\mathbf{K}}{2}\right) - \omega^-\left(-\boldsymbol{l}+\frac{\mathbf{K}}{2}\right), \tag{29}$$

with

$$C = C(\widetilde{\Omega}_K^m) = \frac{A}{1+B}, \quad A = \int \frac{d^3l}{(2\pi)^3}\frac{E(\boldsymbol{l},\mathbf{K})}{\delta\widetilde{\Omega}(\boldsymbol{l},\mathbf{K})}\Psi_0(l), \tag{30}$$

$$B = -\int \frac{d^3l}{(2\pi)^3}\frac{f(\boldsymbol{l},\mathbf{K})}{\delta\widetilde{\Omega}(\boldsymbol{l},\mathbf{K})}W_{12}(l),$$

and

$$E(\boldsymbol{l},\mathbf{K}) = \delta\widetilde{\Omega}(\boldsymbol{l},\mathbf{K}) + \left(\epsilon_0^m + \frac{l^2}{M_x}\right)f(\boldsymbol{l},\mathbf{K}). \tag{31}$$

Here, $\epsilon_0^m = 1.0$ and Ψ_0 are the m binding energy and wave function of Eq. (19), respectively. For the chosen value of $W_{12}(0) = -54\pi$, the Ritz approximation of Ψ_0 gives

$$\Psi_0(l) = \frac{8\sqrt{\pi}}{(l^2+1)^2} \sim W_{12}(l). \tag{32}$$

This property $[\Psi_0(l) \sim W_{12}(l)]$ is crucial for the solution of Eq. (20) given by Eqs. (27) and (28). In Eqs. (26)–(32) we use the usual dimensionless units, the 3D m Rydberg and the 3D m radius, adopted to the m wave equation (19).

The transcendent Eq. (28) with the complex function $C = C(\widetilde{\Omega}_K^m)$ determines self-consistently both the radiative width $\widetilde{\Gamma}^m$ and the m Lamb shift Δ^m, i.e., both the real and imaginary polariton corrections to $\Omega_K^{m(0)}$ of Eq. (19). Because these radiative corrections are small compared to the unperturbed binding energy ϵ_0^m, one can put $C = C(\Omega_K^{m(0)})$. Due to the polariton dispersion, the center-of-mass motion in bipolariton Eq. (20) cannot be split off. As a result, the total m momentum $\mathbf{K}$ influences on the relative motion of the two quasibound polaritons, i.e., $\widetilde{\Psi}(\boldsymbol{l},\mathbf{K})$, $\Delta^m(K)$, and $\widetilde{\Gamma}^m(K)$ are K dependent. The bipolariton wave function $\widetilde{\Psi}$ of Eq. (20) is connected to m Ψ_m of Eq. (6) by the relationship $\widetilde{\Psi}(\boldsymbol{l},\mathbf{K}) = f(\boldsymbol{l},\mathbf{K})\Psi_m(\boldsymbol{l},\mathbf{K})$.

In our analysis of the bipolariton wave equation (20) we simplify the x-x attraction potential W_{12}, but treat the polariton effects exactly. The deuteron model potential of Eq. (26) is often used in biexciton physics.[1,3,15]

Expressing $\sum_{\mathbf{q}} W_{12}(q)\widetilde{\Psi}(\frac{\mathbf{p}-\mathbf{k}}{2}-\mathbf{q})$ from Eq. (20), one receives from Eqs. (18), (16), and (8) the final formula:

$$\chi(\mathbf{p},\omega;\mathbf{k},\omega_{\mathbf{k}},I_{\mathbf{k}}) = \frac{\varepsilon_0}{4\pi}\omega_{\ell t}\frac{\nu^m(\mathbf{p},\mathbf{k},\omega+\omega_{\mathbf{k}})}{\nu^x(\mathbf{p},\mathbf{k},\omega)\nu^m(\mathbf{p},\mathbf{k},\omega+\omega_{\mathbf{k}}) - |M_2^{\rm eff}(\mathbf{p},\mathbf{k})|^2|\mathcal{P}_{\mathbf{k}}|^2}, \tag{33}$$

where

$$\nu^m(\mathbf{p},\mathbf{k},\omega+\omega_{\mathbf{k}}) = \widetilde{\Omega}_{\mathbf{p}+\mathbf{k}}^m + \delta_{\mathbf{p}+\mathbf{k}}^m - \omega - \omega_k - \frac{i}{2}\widetilde{\Gamma}^m(\mathbf{p}+\mathbf{k}), \tag{34}$$

$$\nu^x(\mathbf{p},\mathbf{k},\omega) = \omega^x(p) + \delta_{\mathbf{p}}^x - \omega, \tag{35}$$

with

$$\delta^x_{\mathbf{p}} = \mid \mathcal{P}_{\mathbf{k}} \mid^2 W_{12}(0) \ , \quad \delta^m_{\mathbf{p}+\mathbf{k}} = \mid \mathcal{P}_{\mathbf{k}} \mid^2 \left[W_{12}(0) + W_{22}(0) + \sum_l \mid \Psi(l) \mid^2 W_{22}\left(-l + \frac{\mathbf{p}-\mathbf{k}}{2}\right)\right] . \tag{36}$$

The effective matrix element $M_2^{\rm eff}(\mathbf{p},\mathbf{k})$ of x-x attraction is given by

$$M_2^{\rm eff}(\mathbf{p},\mathbf{k}) = -\left[\epsilon^m_{\rm eff}(\mathbf{p}+\mathbf{k}) + \frac{(\mathbf{p}-\mathbf{k})^2}{4M_x}\right]\Psi_0\left(\frac{\mathbf{p}-\mathbf{k}}{2}\right) , \tag{37}$$

where

$$\epsilon^m_{\rm eff}(\mathbf{p}+\mathbf{k}) = \epsilon^m_0 - \Delta^m(\mathbf{p}+\mathbf{k}) + \frac{i}{2}\,\widetilde{\Gamma}^m(\mathbf{p}+\mathbf{k}) \tag{38}$$

is the complex m effective binding energy renormalized by the polariton effects, i.e., the bipolariton binding energy. In the final expressions for the frequency factors of Eqs. (34) and (35) we include also the nonresonant transient shifts $\delta^x_{\mathbf{p}}$ and $\delta^m_{\mathbf{p}+\mathbf{k}}$ of the x and m levels due to the x-x interaction given by the normal diagram of Fig. 3(a).

Equation (33) gives the total x susceptibility within the exactly solvable bipolariton model with the x-x deuteron attraction potential of Eq. (26). Within our model, the m parameters of Eq. (33), $\Delta^m(\mathbf{p}+\mathbf{k})$ and $\widetilde{\Gamma}^m(\mathbf{p}+\mathbf{k})$, are determined explicitly by Eqs. (28) and (30). The only input m parameter that we need to evaluate the nonlinear susceptibility χ is the unperturbed m binding energy ϵ^m_0 of Eq. (19). The most important consequence of the exact result in comparison with our previous approach[21] is an appearance of the m radiative width $\widetilde{\Gamma}^m$ in Eq. (33). This radiative width is not a phenomenological parameter but is determined self-consistently within the x-γ-m dynamical system. We receive also the renormalized matrix element $M_2^{\rm eff}(\mathbf{p},\mathbf{k})$ of Eq. (37), which corresponds to $M_2(\mathbf{p},\mathbf{k})$ of Eq. (4) with $\epsilon^m = \epsilon^m_{\rm eff}$.

Subtracting the linear contribution

$$\chi_0(\mathbf{p},\omega) = \frac{\varepsilon_0}{4\pi}\,\frac{\omega_{\ell t}}{\omega^x(p)-\omega} \tag{39}$$

from the total x susceptibility of Eq. (33) we find according to Eq. (14) the total m nonlinear susceptibility:

$$\chi^{\rm odd}_{\rm nl}(\mathbf{p},\omega;\mathbf{k},\omega_{\mathbf{k}},I_{\mathbf{k}}) = \frac{\varepsilon_0}{4\pi}\omega_{\ell t}\frac{\mid M_2^{\rm eff}(\mathbf{p},\mathbf{k})\mid^2 \mid \mathcal{P}_{\mathbf{k}}\mid^2}{\nu^x(\mathbf{p},\mathbf{k},\omega)\left[\nu^x(\mathbf{p},\mathbf{k},\omega)\nu^m(\mathbf{p},\mathbf{k},\omega+\omega_{\mathbf{k}}) - \mid M_2^{\rm eff}(\mathbf{p},\mathbf{k})\mid^2 \mid \mathcal{P}_{\mathbf{k}}\mid^2\right]} . \tag{40}$$

In Eqs. (33), (39), and (40) we use the resonant approximation of the x-γ transition. In this approximation $\chi_0(\omega,\mathbf{p})$ of Eq. (39) corresponds to the polariton dispersion of Eq. (21).

To summarize, for the model deuteron potential W_{12} of the x-x attraction we calculated the exact bipolariton wave function $\widetilde{\Psi}$, which one needs for the total m nonlinear susceptibility χ. Therefore, we completed the bipolariton model for the description of the m-mediated optical nonlinear processes in terms of the resonant polariton-polariton scattering.

C. Nonlinear susceptibilities and two-photon absorption of the exactly-solvable bipolariton model

In this subsection, we formulate the nonlinear m susceptibilities in such a way which allows a direct analysis of the corresponding experiments. The final expressions of the m $\chi^{(3)}$ and two-γ absorption $K^{(2)}$ are calculated within the bipolariton model in the low-intensity limit. For intermediate intensities we estimate the transient pump-induced broadening of the two-γ m absorption line.

In order to adopt Eqs. (33) and (40) to a conventional form, one has to express the concentration $|\mathcal{P}_{\mathbf{k}}|^2$ of the transient x's induced virtually by the pump (x component of the polariton pump) through the intensity $I_{\mathbf{k}}$ of corresponding incident light transmitted into the crystal. The frequency $\omega_{\mathbf{k}}$ is supposed to be in a transparency spectral range below ω_t: $\Omega_c > \omega_t - \omega_{\mathbf{k}} \gg \omega_{\ell t}$. Because $I_{\mathbf{k}} \gg I_0$, the probe does not influence a free polariton propagation of the pump. Then, the frequency of the pump $\omega_{\mathbf{k}} = \omega^-(k)$ and the total electromagnetic intensity $I_{\mathbf{k}}$ is divided into the x and γ components with concentrations given by

$$\begin{aligned}
\mid \mathcal{P}_{\mathbf{k}} \mid^2 &= \frac{1}{V}\langle B_{\mathbf{k}}\rangle\langle B^\dagger_{\mathbf{k}}\rangle \\
&= \varphi^-(\mathbf{k},\omega^-(k))\,\frac{I_{\mathbf{k}}}{\omega_{\mathbf{k}} v^g_{\mathbf{k}}} \\
&= \frac{\Omega_c^2}{\Omega_c^2 + 4(\omega_t-\omega_{\mathbf{k}})^2}\,\frac{I_{\mathbf{k}}}{\omega_{\mathbf{k}} v^g_{\mathbf{k}}} , \\
\mid \mathcal{E}_{\mathbf{k}} \mid^2 &= \frac{1}{V}\langle \alpha_{\mathbf{k}}\rangle\langle \alpha^\dagger_{\mathbf{k}}\rangle \\
&= \left[1-\varphi^-(\mathbf{k},\omega^-(k))\right]\,\frac{I_{\mathbf{k}}}{\omega_{\mathbf{k}} v^g_{\mathbf{k}}} \\
&= \frac{4(\omega_t-\omega_{\mathbf{k}})^2}{\Omega_c^2 + 4(\omega_t-\omega_{\mathbf{k}})^2}\,\frac{I_{\mathbf{k}}}{\omega_{\mathbf{k}} v^g_{\mathbf{k}}} ,
\end{aligned} \tag{41}$$

where $v^g_{\mathbf{k}}$ is the polariton group velocity at the frequency $\omega_{\mathbf{k}}$. This group velocity can be found from the dispersion equation (21):

$$v^g_{\mathbf{k}} = \frac{c}{\sqrt{\varepsilon_0}}\eta(\omega_{\mathbf{k}})\,\frac{4(\omega_t-\omega_{\mathbf{k}})^2}{\Omega_c^2 + 4(\omega_t-\omega_{\mathbf{k}})^2} . \tag{42}$$

From Eqs. (41) and (42) one receives the final expressions:

$$| \mathcal{P}_{\mathbf{k}} |^2 = \frac{I_{\mathbf{k}}}{\omega_{\mathbf{k}}} \frac{\sqrt{\varepsilon_0}}{c} \frac{1}{\eta(\omega_{\mathbf{k}})} \frac{\Omega_c^2}{4(\omega_t - \omega_{\mathbf{k}})^2} , \quad (43)$$

$$| \mathcal{E}_{\mathbf{k}} |^2 = \frac{I_{\mathbf{k}}}{\omega_{\mathbf{k}}} \frac{\sqrt{\varepsilon_0}}{c} \frac{1}{\eta(\omega_{\mathbf{k}})} . \quad (44)$$

In Eqs. (42) and (44) the frequency-dependent factor η is given by

$$\eta(\omega_{\mathbf{k}}) = \left[1 + \frac{\omega_{\ell t}}{\omega_t - \omega_{\mathbf{k}}}\right]^{1/2} . \quad (45)$$

Equations (43) and (44) show a cancellation of the polariton effects for the pump components. Apart from the factor $\eta(\omega_{\mathbf{k}}) \simeq 1$, the x resonance does not influence the γ component of Eq. (44), while Eq. (43) for the x component corresponds to second-order perturbation theory.

Equation (40) with $| \mathcal{P}_{\mathbf{k}} |^2$ given by Eq. (43) is the final expression for the total m nonlinear susceptibility $\chi_{\rm nl}^{\rm odd}(\mathbf{p}, \omega; \mathbf{k}, \omega_{\mathbf{k}}, I_{\mathbf{k}})$ within the exactly solvable bipolariton model. Our analysis implies a *coherent* pump. In a general case, $\chi_{\rm nl}^{\rm odd}$ is sensitive to photon statistics of the pump. According to Eq. (15), only the lowest-order contribution to $\chi_{\rm nl}^{\rm odd}$, i.e., $\chi^{(3)}(\omega; \omega_{\mathbf{k}}, -\omega_{\mathbf{k}}, \omega)$, is independent of statistics. A high-intensity limit of the pump, which corresponds to the x-m optical Stark effect (in alternative terms—the x-m transient spectra renormalization[7,8] or the x-m Autler-Townes effect[16]), deals with the whole expression of Eq. (40) without its reduction with Eq. (15) to a few of the low-odd-order nonlinear susceptibilities. This is because the resonant denominator of Eq. (40) includes an intensity-dependent contribution (see also the discussion in Ref. 30). For CuCl, a high-intensity limit corresponds to $I_{\mathbf{k}} \geq I_h = 100$ kW/cm^2. For these intensities the transient renormalizations of x and m spectra are not screened by the m damping $\widetilde{\Gamma}^m$. In the further analysis, we will concentrate on a low-intensity limit.

In the low-intensity limit, one receives from Eqs. (40), (43), and (15) the third-order nonlinear susceptibility $\chi^{(3)}$ and the two-γ absorption coefficient $K^{(2)}$ due to an m:

$$\chi^{(3)}(\omega = \omega; \omega_{\mathbf{k}}, -\omega_{\mathbf{k}}, \omega) = \frac{\varepsilon_0^{3/2}}{32\pi^2} \frac{1}{\eta(\omega)\eta(\omega_{\mathbf{k}})} \frac{\omega_{\ell t}^2}{(\omega_t - \omega)^2(\omega_t - \omega_{\mathbf{k}})^2} \frac{| \epsilon_{\rm eff}^m(\mathbf{p}+\mathbf{k}) + \frac{(\mathbf{p}-\mathbf{k})^2}{4M_x} |^2 \; | \Psi_0\left(\frac{\mathbf{p}-\mathbf{k}}{2}\right) |^2}{\widetilde{\Omega}_{\mathbf{p}+\mathbf{k}}^{m(0)} - \omega - \omega_{\mathbf{k}} - \frac{i}{2}\widetilde{\Gamma}^m(\mathbf{p}+\mathbf{k})} , \quad (46)$$

$$K^{(2)}(\omega, \omega_{\mathbf{k}}) = \frac{\varepsilon_0}{2\hbar c^2} \frac{\sqrt{\omega\omega_{\mathbf{k}}}}{\eta(\omega)\eta(\omega_{\mathbf{k}})} \frac{\omega_{\ell t}^2}{(\omega_t - \omega)^2(\omega_t - \omega_{\mathbf{k}})^2} \times \left|\epsilon_{\rm eff}^m(\mathbf{p}+\mathbf{k}) + \frac{(\mathbf{p}-\mathbf{k})^2}{4M_x}\right|^2 \left|\Psi_0\left(\frac{\mathbf{p}-\mathbf{k}}{2}\right)\right|^2 \frac{\frac{1}{2}\widetilde{\Gamma}^m(\mathbf{p}+\mathbf{k})}{(\widetilde{\Omega}_{\mathbf{p}+\mathbf{k}}^{m(0)} - \omega - \omega_{\mathbf{k}})^2 + \frac{1}{4}[\widetilde{\Gamma}^m(\mathbf{p}+\mathbf{k})]^2} , \quad (47)$$

where $\widetilde{\Omega}_{\mathbf{p}+\mathbf{k}}^{m(0)} = \mathrm{Re}\, \widetilde{\Omega}_{\mathbf{p}+\mathbf{k}}^m = \Omega_{\mathbf{p}+\mathbf{k}}^{m(0)} + \Delta(\mathbf{p}+\mathbf{k})$ and $\eta(\omega)$ is given by Eq. (45). These final expressions are given in the standard dimensional units. The two-γ absorption coefficient $K^{(2)}$ and the third-order nonlinear susceptibility $\chi^{(3)}$ are connected through the relation[31]

$$K^{(2)}(\omega, \omega_{\mathbf{k}}) = \frac{16\pi^2}{c^2\sqrt{\varepsilon_0}} \sqrt{\omega\omega_{\mathbf{k}}} \times \mathrm{Im}\, \chi^{(3)}(\omega = \omega; \omega_{\mathbf{k}}, -\omega_{\mathbf{k}}, \omega) . \quad (48)$$

The nonresonant shifts $\delta_{\mathbf{p}}^x$ and $\delta_{\mathbf{p}+\mathbf{k}}^m$ do not contribute to $K^{(2)}$ and $\chi^{(3)}$.

Equation (46) for $\chi^{(3)}$ is already adopted to the *external* incident and scattered light fields. Corrections due to reflection from the crystal surfaces are not included in Eqs. (46) and (47). They depend on a concrete experimental geometry. These corrections can lead to the additional factors $\eta(\omega)$ and $\eta(\omega_{\mathbf{k}})$ in Eqs. (46) and (47) because the refraction index due to the x resonance is $n_x(\omega) = \sqrt{\varepsilon_0}\eta(\omega)$. For $| \omega_t - \omega |, | \omega_t - \omega_{\mathbf{k}} | \gg \omega_{\ell t}$ one can put $\eta(\omega) = \eta(\omega_{\mathbf{k}}) = 1$. In Eqs. (46) and (47), we neglect both the x spatial dispersion and the x incoherent damping Γ^x. This assumption is valid for $\omega_t - \omega \gg \delta$ or $\omega - \omega_\ell \gg \delta$, where $\delta = \mathrm{Max}\{k^2/2M_x, p^2/2M_x, \Gamma^x\}$ and $\omega_\ell = \omega_t + \omega_{\ell t}$. For CuCl, $\delta \leq 50$ μeV for temperatures $T \leq 10$ K.

Both fundamental interactions of the Hamiltonian (5), the x-γ polariton coupling and the x-x Coulombic attraction, enter into Eqs. (46) and (47) as well as into the general expressions of Eq. (40). With the potential of Eq. (26), the considered exactly solvable model of resonant polariton-polariton scattering treats these basic interactions beyond perturbation theory. Now, the two-γ absorption of Eq. (47) can be interpreted in terms of a resonant cross section $\sigma_{\text{pol-pol}}^m(\mathbf{p}, \mathbf{k})$ of polariton-polariton scattering. The m resonant factor of this cross section is

$$\sigma_{\text{pol-pol}}^m(\mathbf{p}, \mathbf{k}) \sim \frac{\frac{1}{2}\widetilde{\Gamma}^m(\mathbf{p}+\mathbf{k})}{(\widetilde{\Omega}_{\mathbf{p}+\mathbf{k}}^{m(0)} - \omega - \omega_{\mathbf{k}})^2 + \frac{1}{4}[\widetilde{\Gamma}^m(\mathbf{p}+\mathbf{k})]^2} . \quad (49)$$

Equation (49) is consistent with a basic requirement of the general theory of resonant scattering.[20] This resonant factor enters into Eqs. (46) and (47). The spectral width of the m resonant cross section given by $\widetilde{\Gamma}^m(\mathbf{p}+\mathbf{k})$ of Eq. (28) equals the inverse radiative lifetime of a metastable m "ground state." Actually, the resonant cross section $\sigma_{\text{pol-pol}}^m(\mathbf{p}, \mathbf{k})$ describes both the mutually inverse processes – m absorption and m optical decay [polariton($\mathbf{p}$) + polariton($\mathbf{k}$) $\leftrightarrow$ $m(\mathbf{p}+\mathbf{k})$].

Equation (47) is valid in a low-intensity limit, in which the intensity of the pump wave $I_{\mathbf{k}} \leq I_\ell$ is so small that the two interacting polariton waves are similar (for CuCl $I_\ell \simeq$ 10 kW/cm^2). As a result, Eq. (47) is symmetric with respect to $(\mathbf{p},\omega) \leftrightarrow (\mathbf{k},\omega_{\mathbf{k}})$. However, one can apply Eq. (40) with Eq. (43) for the intermediate pump intensities $I_\ell \leq I_{\mathbf{k}} \leq I_h$. For these intensities, the transient x-m splitting induced by the pump is still not well developed, while the m absorption Lorentzian of Eq. (47) already undergoes a power broadening caused by the pump.[16] For this regime, one gets for the two-γ m absorption the following change in Eq. (47):

$$\frac{\frac{1}{2}\Gamma^m}{(\Omega^m-\omega-\omega_{\mathbf{k}})^2+\frac{1}{4}(\Gamma^m)^2} \longrightarrow \frac{\frac{1}{2}\Gamma^m}{\left[(\Omega^m-\omega-\omega_{\mathbf{k}})^2+\frac{1}{4}(\Gamma^m)^2\right]^{1/2}\left[(\Omega^m-\omega-\omega_{\mathbf{k}})^2+a(I_{\mathbf{k}})\Gamma^m+\frac{1}{4}(\Gamma^m)^2\right]^{1/2}}, \tag{50}$$

where $\Gamma^m = \widetilde{\Gamma}^m(\mathbf{p}+\mathbf{k})$, $\Omega^m = \widetilde{\Omega}^{m(0)}_{\mathbf{p}+\mathbf{k}}$, and the dimensionless field-dependent parameter $a = a(I_{\mathbf{k}})$ is

$$a(I_{\mathbf{k}}) = \frac{\omega_{\ell t}^2}{2(\omega_\ell-\omega)(\omega_t-\omega)}\frac{\sqrt{\varepsilon_0}}{c} I_{\mathbf{k}} \frac{|M_2^{\rm eff}(\mathbf{p},\mathbf{k})|^2}{(\omega_t-\omega_{\mathbf{k}})^2\,\Gamma^m}. \tag{51}$$

Here $M_2^{\rm eff}(\mathbf{p},\mathbf{k})$ is given by Eq. (37). For $I_{\mathbf{k}} \to 0$, the field-dependent parameter $a \to 0$ and the right-hand side of Eq. (50) transform to a Lorentzian. In order to estimate analytically the radiative pump-induced broadening we approximate the right-hand side of Eq. (50) by the following ansatz:

$$\frac{\Gamma^m}{\Gamma^m_{\rm eff}(I_{\mathbf{k}})}\frac{\frac{1}{2}\Gamma^m_{\rm eff}(I_{\mathbf{k}})}{(\Omega^m-\omega-\omega_{\mathbf{k}})^2+\frac{1}{4}[\Gamma^m_{\rm eff}(I_{\mathbf{k}})]^2}, \tag{52}$$

where the effective m broadening is

$$\begin{aligned}\Gamma^m_{\rm eff}(I_{\mathbf{k}}) &= \left[\int \frac{\pi\ d\omega}{\left[(\Omega^m-\omega-\omega_{\mathbf{k}})^2+\frac{1}{4}(\Gamma^m)^2\right]^{1/2}\left[(\Omega^m-\omega-\omega_{\mathbf{k}})^2+a(I_{\mathbf{k}})\Gamma^m+\frac{1}{4}(\Gamma^m)^2\right]^{1/2}}\right]^{-1} \\ &= \frac{\pi}{2}\sqrt{1+a(I_{\mathbf{k}})}\,K\left(\frac{\sqrt{2a(I_{\mathbf{k}})}}{\sqrt{1+a(I_{\mathbf{k}})}}\right)^{-1}\Gamma^m.\end{aligned} \tag{53}$$

Here, $K(x)$ is the complete elliptic integral. If $a(I_{\mathbf{k}}) \ll 1$, one can further approximate:

$$\Gamma^m_{\rm eff}(I_{\mathbf{k}}) \simeq \Gamma^m\left[1+\frac{3}{8}a^2(I_{\mathbf{k}})\right]. \tag{54}$$

The effective Lorentzian of Eq. (52) with $\Gamma^m_{\rm eff}$ of Eqs. (53) and (54) shows how the pump-induced broadening approaches the low-intensity limit with decreasing $I_{\mathbf{k}}$.

In this subsection we calculated within the bipolariton model the m $\chi^{(3)}$ and $K^{(2)}$ and prepared our results for a comparison with experimental measurements.

III. BIEXCITON NONLINEAR OPTICAL RESPONSE OF THE GIANT OSCILLATOR STRENGTH MODEL

In this section we describe briefly the giant oscillator strength model and calculate with this model the m-mediated χ, $\chi^{(3)}$, and $K^{(2)}$ for a direct comparison with the bipolariton model.

The giant oscillator strength model of Eq. (1) deals with the following model Hamiltonian:

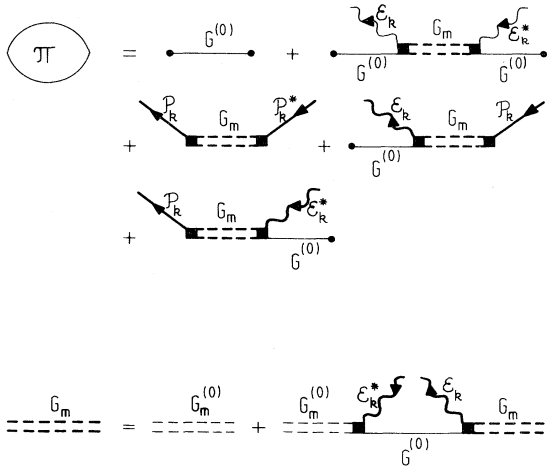

FIG. 4. Giant oscillator strength model. Diagram equations for the polarization operator Π of the probe field. The large bold squares are ascribed to the matrix element M_1 of the optical conversion $x+\gamma \leftrightarrow m$, $G^{(0)}_m$ and G_m are the free m Green function determined by the m operators $A_{\mathbf{K}}$ of the model Hamiltonian (55) and the m Green function renormalized by the pump wave, respectively.

$$H=\sum_{\sigma,\mathbf{p}}\Big[\ \omega^{x}(p)B^{\dagger}_{\sigma\mathbf{p}}B_{\sigma\mathbf{p}}\ +\ \omega^{\gamma}(p)\alpha^{\dagger}_{\sigma\mathbf{p}}\alpha_{\sigma\mathbf{p}}\ +\ \Omega^{m}_{\mathbf{p}}A^{\dagger}_{\mathbf{p}}A_{\mathbf{p}}+\frac{i\Omega_c}{2}\left(\alpha^{\dagger}_{\sigma\mathbf{p}}B_{\sigma\mathbf{p}}\ -\ B^{\dagger}_{\sigma\mathbf{p}}\alpha_{\sigma\mathbf{p}}\right)$$
$$+\sum_{l}\ \frac{1}{\sqrt{V}}M_1(\mathbf{p},l)\ \left(A^{\dagger}_{\mathbf{p}+l}\alpha_{\sigma\mathbf{p}}B_{\sigma\neq\sigma' l}-A_{\mathbf{p}+l}B^{\dagger}_{\sigma\neq\sigma' l}\alpha^{\dagger}_{\sigma\mathbf{p}}\right)\ \Big]\ . \tag{55}$$

The matrix element $M_1(\mathbf{p},\mathbf{k})$ of Eqs. (2) and (55) is derived within a perturbation theory as $M_1(\mathbf{p},\mathbf{k})=\sum_{\sigma_1,l}\langle 0|A^{\dagger}_{\mathbf{p}+l}[-i\frac{\Omega_c}{2}B^{\dagger}_{\sigma_1 l}\alpha_{\sigma_1 l}]B^{\dagger}_{\sigma\neq\sigma_1\mathbf{p}}\alpha^{\dagger}_{\sigma\mathbf{k}}|0\rangle$. This construction corresponds to the optical conversion $x+\gamma\leftrightarrow m$.

The model Hamiltonian of Eq. (55) is inconsistent with the underlying e-h-γ picture, as well as with the x-γ Hamiltonian of Eq. (55).[21] Equation (55) deals with a considerably symplified physical picture and masks the important features of the resonant polariton-polariton scattering which is responsible for two-γ m generation. With the Hamiltonian of Eq. (55) one obtains the often used results for $\chi^{\rm odd}_{\rm nl}$, $\chi^{(3)}$, and $K^{(2)}$. The corresponding diagrams are shown in Fig. 4.

Apart from the other matrix element (M_1) attributed to the large bold square dots, the equations of Figs. 2 and 4 have also different diagram blocks. For example, the diagram equations of Fig. 4 contain wavy lines due to the electric component $\mathcal{E}_{\mathbf{k}}$ of the pump wave. These lines are absent in Fig. 2 because the proper matrix element $M_2(\mathbf{p},\mathbf{k})$ involves for an m creation only the x components of two interacting polaritons. In comparison with the analysis of the giant oscillator strength model given in Refs. 4, 6–9, and 21, we include also the *interference* terms $\sim(\mathcal{E}_{\mathbf{k}}\mathcal{P}^{*}_{\mathbf{k}}+\text{H.c.})$. These terms are shown by the last two graphs of the first diagram equation of Fig. 4. They contribute to the total $\chi^{(3)}$, if $\mid\omega_t-\omega_{\mathbf{k}}\mid\gg\Gamma^{x}$.

The diagram equations of Fig. 4 result in the following expression for $\chi^{\rm odd}_{\rm nl}$:

$$\chi^{\rm odd}_{\rm nl}(\mathbf{p},\omega;\mathbf{k},\omega_{\mathbf{k}},I_{\mathbf{k}})=\frac{\varepsilon_0}{2\pi\omega_t}\left[\frac{\Omega_c}{2}\mathcal{E}_{\mathbf{k}}+\nu^{x}_0(\mathbf{p},\omega)\mathcal{P}_{\mathbf{k}}\right]\left[\frac{\Omega_c}{2}\mathcal{E}^{*}_{\mathbf{k}}+\nu^{x}_0(\mathbf{p},\omega)\mathcal{P}^{*}_{\mathbf{k}}\right]$$
$$\times\frac{\mid M_1(\mathbf{p},\mathbf{k})\mid^2}{\nu^{x}_0(\mathbf{p},\omega)\left[\nu^{x}_0(\mathbf{p},\omega)\nu^{m}_0(\mathbf{p},\mathbf{k},\omega+\omega_{\mathbf{k}})-\mid M_1(\mathbf{p},\mathbf{k})\mid^2\mid\mathcal{E}_{\mathbf{k}}\mid^2\right]}\ , \tag{56}$$

where the electric field $\mathcal{E}_{\mathbf{k}}$ and polarization $\mathcal{P}_{\mathbf{k}}$ components of the pump are given by Eqs. (43) and (44) and

$$\nu^{m}_0(\mathbf{p},\mathbf{k},\omega+\omega_{\mathbf{k}})\ =\ \Omega^{m}_{\mathbf{p}+\mathbf{k}}-\omega-\omega_k-\frac{i}{2}\Gamma^{m}(\mathbf{p}+\mathbf{k})\ , \tag{57}$$
$$\nu^{x}_0(\mathbf{p},\omega)\ =\ \omega^{x}(p)-\omega\ . \tag{58}$$

In comparison with Eqs. (34) and (35), Eqs. (57) and (58) do not include the nonresonant x and m shifts. In the low-intensity limit, Eq. (56) reduces to

$$\chi^{(3)}(\omega=\omega;\omega_{\mathbf{k}},-\omega_{\mathbf{k}},\omega)\ =\ \frac{\varepsilon_0^{3/2}}{32\pi^2}\ \frac{1}{\eta(\omega)\eta(\omega_{\mathbf{k}})}\ \frac{\omega^2_{\ell t}}{(\omega_t-\omega)^2(\omega_t-\omega_{\mathbf{k}})^2}\ \frac{(2\omega_t-\omega-\omega_{\mathbf{k}})^2\ \mid\Psi_m\left(\frac{\mathbf{p}-\mathbf{k}}{2}\right)\mid^2}{\Omega^{m}_{\mathbf{p}+\mathbf{k}}-\omega-\omega_{\mathbf{k}}-\frac{i}{2}\Gamma^{m}(\mathbf{p}+\mathbf{k})}\ , \tag{59}$$

$$K^{(2)}(\omega,\omega_{\mathbf{k}})\ =\ \frac{\varepsilon_0}{2\hbar c^2}\ \frac{\sqrt{\omega\omega_{\mathbf{k}}}}{\eta(\omega)\eta(\omega_{\mathbf{k}})}\ \frac{\omega^2_{\ell t}}{(\omega_t-\omega)^2(\omega_t-\omega_{\mathbf{k}})^2}(2\omega_t-\omega-\omega_{\mathbf{k}})^2$$
$$\times\left|\Psi_m\left(\frac{\mathbf{p}-\mathbf{k}}{2}\right)\right|^2\ \frac{\frac{1}{2}\Gamma^{m}(\mathbf{p}+\mathbf{k})}{(\Omega^{m}_{\mathbf{p}+\mathbf{k}}-\omega-\omega_{\mathbf{k}})^2+\frac{1}{4}[\Gamma^{m}(\mathbf{p}+\mathbf{k})]^2}\ . \tag{60}$$

The general expressions of Eqs. (40) and (56) as well as the corresponding Eqs. (46) and (47) and Eqs. (59) and (60) for $\chi^{(3)}$ and $K^{(2)}$ are different. In comparison, they contain different frequency-dependent factors. These differences can be tested experimentally. However, at first one should define the m energy Ω^{m}_{K}, wave function Ψ_m, and radiative width Γ^{m} in Eqs. (56) and (60). These m parameters and functions cannot be derived self-consistently from the model Hamiltonian (55).

The most natural way to complete the treatment within Eqs. (56), (59), and (60) is to apply the bipolariton wave equation (20) and to put $\Omega^{m}_{\mathbf{p}+\mathbf{k}}=\widetilde{\Omega}^{m(0)}_{\mathbf{p}+\mathbf{k}}$, $\Gamma^{m}(\mathbf{p}+\mathbf{k})=\widetilde{\Gamma}^{m}(\mathbf{p}+\mathbf{k})$, and $\Psi_m[(\mathbf{p}-\mathbf{k})/2]=\widetilde{\Psi}(\mathbf{p},\mathbf{k})/f(\mathbf{p},\mathbf{k})$. This gives for two-$\gamma$ m absorption of Eq. (60)

$$K^{(2)}(\omega,\omega_{\mathbf{k}})=\frac{\varepsilon_0}{2\hbar c^2}\ \frac{\sqrt{\omega\omega_{\mathbf{k}}}}{\eta(\omega)\eta(\omega_{\mathbf{k}})}\ \frac{\omega^2_{\ell t}}{(\omega_t-\omega)^2(\omega_t-\omega_{\mathbf{k}})^2}\ (2\omega_t-\omega-\omega_{\mathbf{k}})^2$$
$$\times\left|\epsilon^{m}_{\rm eff}(\mathbf{p}+\mathbf{k})+\frac{(\mathbf{p}-\mathbf{k})^2}{4M_x}\right|^2\left|\Psi_0\left(\frac{\mathbf{p}-\mathbf{k}}{2}\right)\right|^2\ \frac{\frac{1}{2}\widetilde{\Gamma}^{m}(\mathbf{p}+\mathbf{k})}{\left[(\widetilde{\Omega}^{m(0)}_{\mathbf{p}+\mathbf{k}}-\omega-\omega_{\mathbf{k}})^2+\frac{1}{4}[\widetilde{\Gamma}^{m}(\mathbf{p}+\mathbf{k})]^2\right]^2}\ . \tag{61}$$

Now, all the parameters of Eq. (61) are determined. However, Eq. (61) yields a non-Lorentzian m absorption line. Moreover, Eqs. (47) and (61) give different frequency dependences of the integrated two-γ absorption coefficient $\sigma^{(2)}(\omega) = \int K^{(2)}(\omega, \omega_{\mathbf{k}}) d\omega_{\mathbf{k}}$. Although the integration over the frequency $\omega_{\mathbf{k}}$ removes the different resonant factors in Eqs. (47) and (61), the different frequency dependences of $\sigma^{(2)}(\omega)$ within the two models are still present due to the implicit dependence $\widetilde{\Gamma}^m = \widetilde{\Gamma}^m[\mathbf{p}(\omega) + \mathbf{k}(\omega_{\mathbf{k}})]$. Here, $p = p(\omega)$ and $k = k(\omega_{\mathbf{k}})$ follow the polariton dispersion of Eq. (21).

Another possibility to analyze Eqs. (56), (59), and (60) is to use the m wave equation (19) unperturbed by the polariton effects. Then, one has to put $\Psi_m[(\mathbf{p} - \mathbf{k})/2] = \Psi_0[(\mathbf{p} - \mathbf{k})/2]$ and $\Omega^m_{\mathbf{p}+\mathbf{k}} = \Omega^{m(0)}_{\mathbf{p}+\mathbf{k}}$. However, in this approach the m radiative width $\Gamma^m(\mathbf{p} + \mathbf{k})$ is still undefined. In order to determine this important m parameter one can treat the m optical decay $m \to x + \gamma$ by the standard second-order perturbation theory:[29]

$$\frac{1}{2}\Gamma^m(\mathbf{K}) = \frac{\pi}{4}\int \frac{d^3p}{(2\pi)^3}\,\Omega_c^2\,|\Psi_0(p)|^2 \times \delta\left(\Omega_K^{m(0)} - \omega^{\pm}\left(\mathbf{p} + \frac{\mathbf{K}}{2}\right) - \omega^{\pm}\left(-\mathbf{p} + \frac{\mathbf{K}}{2}\right)\right). \tag{62}$$

As we discussed above, the resonant polariton-polariton scattering as well as a bipolariton metastable state cannot be treated within the perturbation theory.

In summary, the giant oscillator strength model is formulated to allow a direct comparison with the bipolariton model and with high-precision experiments.

IV. OPTICAL PROPERTIES OF BIEXCITONS IN CuCl: EXPERIMENTAL VERIFICATION OF THE BIPOLARITON MODEL

We examine the following high-precision experimental results: (i) the m radiative width $\Gamma^m(K \simeq 0)$, (ii) the resonant maxima of $\chi^{(3)} = \chi^{(3)}(\omega = \Omega^m_{\mathbf{p}+\mathbf{k}} - \omega_{\mathbf{k}}; \omega_{\mathbf{k}}, -\omega_{\mathbf{k}}, \Omega^m_{\mathbf{p}+\mathbf{k}} - \omega_{\mathbf{k}})$, and (iii) the integrated two-γ absorption line shape $\sigma^{(2)}(\omega) = \int K^{(2)}(\omega, \omega_{\mathbf{k}}) d\omega_{\mathbf{k}}$.

A. Measurements of $\chi^{(3)}$ and Γ^m by high-resolution polarization spectroscopy

For the correct experimental evaluation of the resonant m susceptibility $\chi^{(3)}$ and the radiative width Γ^m in the low-intensity limit $I_{\mathbf{k}} \leq 10$ kW/cm^2, the spectral resolution has to be ≤ 10 μ eV. The experimental setup for high-resolution polarization rotation spectroscopy has been developed in Ref. 18. The UV light source consists of a Ti-sapphire ring laser (Coherent 899-02) and an excimer laser (Lambda 53 EMC), which pump a dye amplifier. An output of the UV light source is given by a frequency doubler ($LiIO_3$ crystal). This UV source generates the circular polarized coherent pump light. The pump pulse duration, its spectral width, and the repetition rate are ~ 10 ns, ~ 1 μ eV, and 10 Hz, respectively. The intensity of the pump light $I_{\mathbf{k}} \simeq 0.5$–$10$ kW/cm^2.

The linear polarized probe light is generated by a usual UV dye laser pumped by the excimer laser. The initial broad spectrum (~ 170 μeV) is reduced to the spectral linewidth of ~ 3 μeV by an air space Fabry-Pérot interferometer (FSR = 225 μeV, finess = 75). The intensity of the probe light $I_0 \simeq 0.18$ kW/cm^2. The photon energy ω ($\hbar = 1$) of the probe light is tuned by a change of the air pressure in the interferometer. The intensity of the probe light transmitted through the sample and a crossed polarizer (analyzer) is measured by a photomultiplier (Hamamatsu R654).

Single-crystal platelets of CuCl, a sample No. 1 with the thickness $d = 9.8$ μm and a sample No. 2 with $d = 22.8$ μm, are held in an immersion-type cryostat at 2 K. We measure the polarization spectrum of the probe light due to the two-γ m resonance as a function of $\omega + \omega_{\mathbf{k}}$. In the present experiment, the photon energy of the pump light $\omega_{\mathbf{k}} = 3.18622$ eV is fixed. In our excitation geometry, the resonant coupling between the counterpropagating pump and probe light involves the m's with $K = k - p = 3 \times 10^3$ cm^{-1}. A very small additional signal is also present due to the interaction between the probe and the pump wave reflected back at the rear surface of the sample. This geometry involves the m's with $K = k + p = 8.85 \times 10^5$ cm^{-1}. However, both signal peaks are well separated in frequency.

The width and the maximum of the resonant polarization signal due to the m's with $K = 3 \times 10^3$ cm^{-1} are shown in Figs. 5(a) and 5(b) and 6(a) and 6(b) as a function of the pump intensity for samples 1 and 2, respectively. The signal intensity is given by[14]

$$J(\omega) = \frac{1}{2}\left|\Delta n(\omega, I_{\mathbf{k}})\; p_0\; d\right|^2, \tag{63}$$

where $\Delta n(\omega, I_{\mathbf{k}})$ is the pump-induced nonlinear change of the complex refractive index between the two mutually opposite circularly polarized components $\sigma^{\pm}$ ($\sigma = 1, 2$) of the probe and p_0 is the wave vector of the probe light outside the sample. Only one of these two components of the linear polarized probe light couples with the circular polarized pump light in the resonant generation of m's. The corresponding resonant m nonlinear susceptibility $\chi^{(3)}$ is connected with $\Delta n(I_{\mathbf{k}})$ by

$$\Delta n(\omega, I_{\mathbf{k}}) = \frac{2\pi}{n_x(\omega)}\chi^{(3)}(\omega = \Omega^m_{k-p} - \omega_{\mathbf{k}}; \omega_{\mathbf{k}}, -\omega_{\mathbf{k}}, \Omega^m_{k-p} - \omega_{\mathbf{k}})\;|\;\mathcal{E}_{\mathbf{k}_0}\;|^2, \tag{64}$$

where $n_x(\omega)$ is the linear polariton refractive index and $\mathcal{E}_{\mathbf{k}_0}$ is the amplitude of the electric field of the incident pump light.

According to Figs. 5(a) and 5(b), the pump-induced broadening of the polarization signal vanishes at the pump intensity $I_{\mathbf{k}} \leq 1$ kW/cm^2. This intensity-independent limit of the width of the m polarization spectra is attributed to the radiative width $\Gamma^m(K)$ of an m. According to Figs. 5(a) and 5(b), the corresponding values are given by $\Gamma^m(K = 3\times10^3\ \text{cm}^{-1}) = 24\pm2\ \mu\text{eV}$ and $36 \pm 3\ \mu$ eV for samples 1 and 2, respectively. The same thresholds on the pump intensity take place for the resonant values of the polarization signal [see Figs. 6(a) and 6(b)]. Namely, only for $I_{\mathbf{k}} \leq 1$ kW/cm^2 can these values be attributed to the corresponding $\chi^{(3)}$. Then, with Eqs. (63) and (64) we estimate $\chi^{(3)}_{\max} = (3.0 \pm 0.9) \times 10^{-4}$ esu and $\chi^{(3)}_{\max} = (1.7 \pm 0.6) \times 10^{-4}$ esu for samples 1 and 2, respectively.

B. Measurements of the two-photon m absorption

The experimental configuration of the two-γ m absorption measurements[32] is shown schematically in Fig. 7. The pump and probe light are linear and circular polarized, respectively. Now, the circular polarized probe light can be decomposed in a coherent superposition of the two components with the mutually orthogonal linear polarizations. According to the selection rules in CuCl, only the component polarized parallel to the polarization of the pump light gives rise to the m pump-probe absorption. The polarized beam splitter (see Fig. 7) allows us to separate each linear polarized component of the transmitted probe. Then, the corresponding intensities $\widetilde{I}_{0,\parallel}$ and $\widetilde{I}_{0,\perp}$ are detected independently by the p-i-n photodiodes (Hamamatsu S3072). The intensities of the pump and probe light are $I_{\mathbf{k}} = 2$–10 kW/cm^2 and $I_0 = 0.4$ kW/cm^2, respectively.

The transmitted intensity $\widetilde{I}_{0,\parallel}$ of the component that interacts resonantly with the pump light is given by

$$\widetilde{I}_{0,\parallel}(\omega,\omega_{\mathbf{k}}) = \tfrac{1}{2} I_0 \exp\left[-\alpha_L(\omega)d - \alpha_{\mathrm{NL}}(\omega,\omega_{\mathbf{k}},I_{\mathbf{k}})d\right] , \tag{65}$$

where $\alpha_L(\omega)$ and $\alpha_{\mathrm{NL}}(\omega,\omega_{\mathbf{k}},I_{\mathbf{k}})$ are the linear polariton absorption and the nonlinear m absorption induced by the pump, respectively. Another linear polarized com-

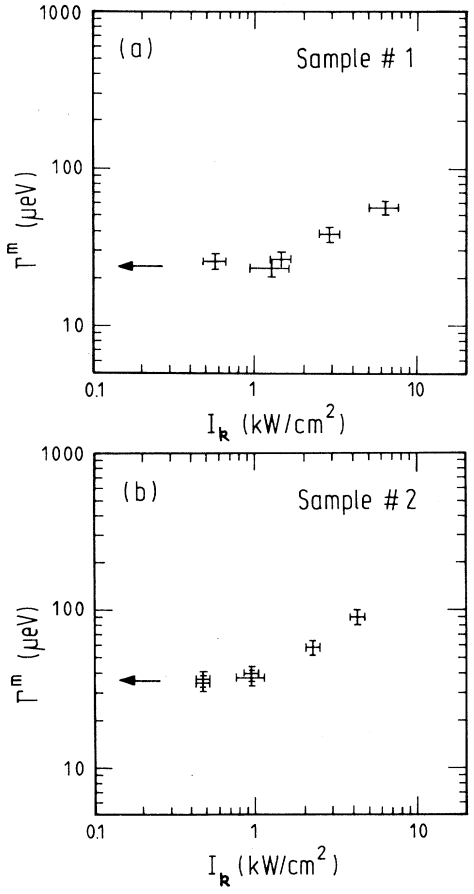

FIG. 5. The spectral width of the m polarization signal of samples 1 (a) and 2 (b) as a function of the pump intensity $I_{\mathbf{k}}$. The counterpropagating pump-probe geometry, the coherently photogenerated m's have the wave vector $K = 3 \times 10^3$ cm^{-1}.

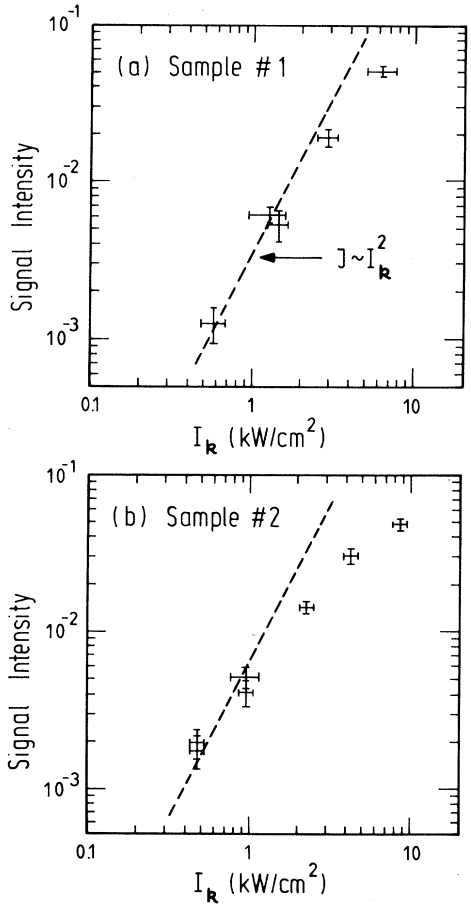

FIG. 6. The maximum of the resonant m polarization signal of samples 1 (a) and 2 (b) vs the pump intensity $I_{\mathbf{k}}$. The pump-probe geometry is the same as in Fig. 5. The dashed line in each figure shows the quadratic law for the eye guide.

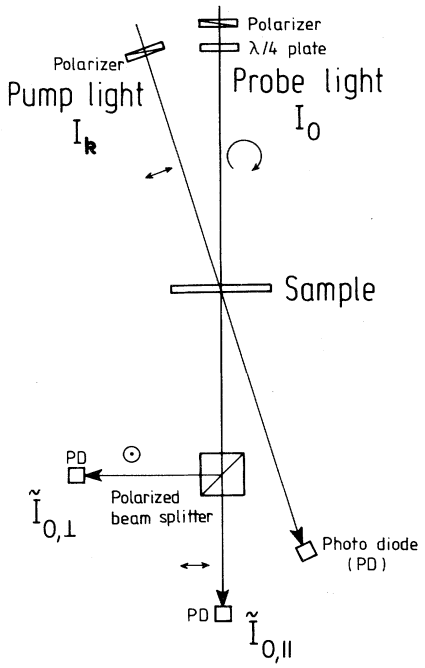

FIG. 7. The experimental configuration for two-γ m absorption spectroscopy.

ponent of the probe undergoes only the linear polariton absorption:

$$\tilde{I}_{0,\perp}(\omega,\omega_{\mathbf{k}}) = \tfrac{1}{2} I_0 \exp\left[-\alpha_L(\omega) d\right] . \tag{66}$$

From Eqs. (65) and (66) one concludes

$$\alpha_{\rm NL}(\omega,\omega_{\mathbf{k}},I_{\mathbf{k}}) = \frac{1}{d} \ln\left(\frac{\tilde{I}_{0,\perp}}{\tilde{I}_{0,\parallel}}\right) , \tag{67}$$

where $\alpha_{\rm NL}(\omega,\omega_{\mathbf{k}},I_{\mathbf{k}})$ is connected with the two-γ m absorption coefficient by the simple relationship

$$\alpha_{\rm NL}(\omega,\omega_{\mathbf{k}},I_{\mathbf{k}}) = \langle I_{\mathbf{k}}\rangle \, K^{(2)}(\omega,\omega_{\mathbf{k}}) . \tag{68}$$

Here, $\langle I_{\mathbf{k}}\rangle$ is the spatially averaged pump intensity inside the crystal:

$$\langle I_{\mathbf{k}}\rangle = I_{\mathbf{k}} \frac{1-e^{-\alpha_L(\omega_{\mathbf{k}})d}}{\alpha_L(\omega_{\mathbf{k}})\, d} . \tag{69}$$

Finally, the two-γ m absorption coefficient $K^{(2)}(\omega,\omega_{\mathbf{k}})$ is evaluated with Eqs. (67)–(69). This method allows us to extract the two-γ absorption from the linear absorption background as well as to avoid an influence of the fluctuations of the probe intensity I_0. These fluctuations are identical for both components, $\tilde{I}_{0,\parallel}$ and $\tilde{I}_{0,\perp}$, and according to Eq. (67) automatically cancel each other. From the measured $K^{(2)}(\omega,\omega_{\mathbf{k}})$ we find the integrated two-γ absorption $\sigma^{(2)}(\omega)$ by the straightforward numerical integration over the frequency $\omega_{\mathbf{k}}$.

In the experiment, photon energies of the probe and pump light satisfy the condition $\omega > \Omega^{m(0)}/2 > \omega_{\mathbf{k}}$ in order to (i) reduce the spatial inhomogeneity of the pump light inside the crystal and (ii) minimize an accumulation of the real x's generated by the pump and probe light due to the background linear and nonlinear optical processes. The experimental dependence of the normalized integrated two-γ m absorption spectra $\tilde{\sigma}^{(2)}(\omega) = \sigma^{(2)}(\omega)/\sigma^{(2)}(\omega = \frac{\Omega^m}{2})$ is shown in Fig. 8 (circle dots).

C. Comparison of the experimental results with the two models

(i) The exactly solvable bipolariton model.—In order to estimate numerically Eqs. (46) and (47) of the exactly solvable model one has to solve Eq. (28). We use $\epsilon_0^m = 34$ meV as the only input m parameter for Eqs. (26)–(32). The corresponding m radius is determined by $\Psi_0(p)$ as $a_m = 9.3$ Å. The following x and polariton parameters of CuCl have been used: $\varepsilon_0 = 5.6$, $\omega_t = 3.2022$ eV, $\omega_{\ell t} = 5.7$ meV, and $M_x = 2.6 m_0$. The dependence $\Gamma^m = \tilde{\Gamma}^m(K)$ as a result of the numerical solution of Eqs. (28)–(31) is shown in Fig. 9 (solid line). The feature of the theoretical curve $\tilde{\Gamma}^m(K)$ at $K = K_0 = 8.85 \times 10^5$ cm^{-1} with a jump of the first derivative is due to the van Hove feature in a joint density of bipolariton states which is determined by the function $\delta\tilde{\Omega}(\mathbf{p},\mathbf{K})$ of Eq. (29) (see also the corresponding discussion in Ref. 22). According to the numerical calculations, $\tilde{\Gamma}^m(K=0) = 27.4$ μeV. Thus, the quantitative agreement between the theoretical and experimental results is rather good, particularly because there is no fitting parameters in the exactly solvable bipolariton model. For comparison, the two experimental points $\Gamma^m(K = 3 \times 10^3$ cm$^{-1})$ are also shown in Fig. 9.

The experimental dependences Γ^m on the pump intensity $I_{\mathbf{k}}$ shown in Figs. 5(a) and 5(b) cannot be attributed to the dynamical transient pump-induced broadening

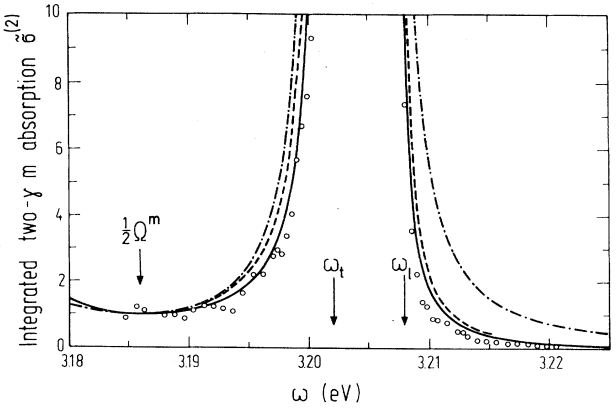

FIG. 8. The normalized integrated two-γ m absorption line shape $\tilde{\sigma}^{(2)}(\omega)$. Circles: the experimental result; solid curves: the bipolariton model; dash-dotted curves: the giant oscillator strength model with the biexciton wave function Ψ_0 of Eq. (19) and without the interference terms; dashed curves: the giant oscillator strength model with the bipolariton wave function $\Psi_m = \tilde{\Psi}/f$ of Eq. (20).

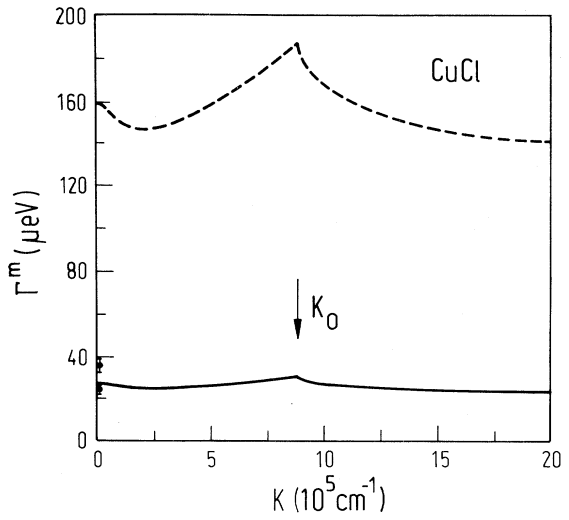

FIG. 9. The dependence of the m radiative width Γ^m on the total m momentum K. Bold points: the experimental values of $\Gamma^m(K = 3\times10^3\ \mathrm{cm}^{-1})$ found from Figs. 6(a) and 6(b); solid line: $\Gamma^m = \widetilde{\Gamma}^m(K)$ of the bipolariton model; dashed line: $\Gamma^m = \Gamma^m(K)$ of the giant oscillator strength model [Eq. (62)].

of Eqs. (53) and (54). The corresponding thresholds $I_\ell \simeq$ 10–30 kW/cm^2 given by the condition $a(I_{\mathbf{k}}) \leq 1$ of Eq. (51) exceed considerably the experimental ones. Thus, we conclude an incoherent, kinetic origin of the pump-induced broadening in Figs. 5(a) and 5(b) due to a stray generation and accumulation of the real x's and m's which influence Γ^m. A still further decrease of the pump pulse duration to a subnanosecond time scale will allow one to avoid this incoherent effect.

From Eq. (46) we estimate the resonant maximum value of $\chi^{(3)}_{\max}$ for $\widetilde{\Omega}^{m(0)}_{\mathbf{p}+\mathbf{k}} - \omega - \omega_{\mathbf{k}} = 0$ as $\chi^{(3)}_{\max} = \chi^{(3)}(\omega = \widetilde{\Omega}^{m(0)}_{\mathbf{p}+\mathbf{k}} - \omega_{\mathbf{k}}; \omega_{\mathbf{k}}, -\omega_{\mathbf{k}}, \widetilde{\Omega}^{m(0)}_{\mathbf{p}+\mathbf{k}} - \omega_{\mathbf{k}}) = 1.05 \times 10^{-4}$ esu. In this estimate, $\omega_{\mathbf{k}}$ is chosen to be the experimental value of 3.18622 eV, which is very close to $\frac{\Omega^m}{2}$. This value of $\chi^{(3)}(\omega = \widetilde{\Omega}^{m(0)}_{\mathbf{p}+\mathbf{k}} - \omega_{\mathbf{k}}; \omega_{\mathbf{k}}, -\omega_{\mathbf{k}}, \widetilde{\Omega}^{m(0)}_{\mathbf{p}+\mathbf{k}} - \omega_{\mathbf{k}})$ obtained within the exactly solvable model is again in rather good quantitative agreement with our experimental results.

The calculated line shape of the normalized integrated two-γ m absorption coefficient $\widetilde{\sigma}^{(2)}(\omega)$ for the bipolariton model is shown in Fig. 8 (solid line). The theoretical curves reproduce the measured line shape within the experimental accuracy. These numerical calculations use Eq. (47) for $K^{(2)}(\omega, \omega_{\mathbf{k}})$. Our experimental scheme (see Fig. 7) for the two-γ m absorption involves the *linear* polarized pump light, while the corresponding self-consistent theory is given for the *circular* polarized pump. As we discussed above, this difference can influence the final expression for the total resonant m nonlinear susceptibility $\chi^{\mathrm{odd}}_{\mathrm{nl}}(\mathbf{p}, \omega; \mathbf{k}, \omega_{\mathbf{k}}, I_{\mathbf{k}})$ of Eq. (14). However, we have checked that in the low-intensity limit of the pump both polarizations give the identical pump-probe $\chi^{(3)}(\omega = \omega; \omega_{\mathbf{k}}, -\omega_{\mathbf{k}}, \omega)$ and $K^{(2)}(\omega, \omega_{\mathbf{k}})$.

Thus, we conclude that the bipolariton model with the scheme of Eq. (3) explains *quantitatively* the high-precision experimental results for $\Gamma^m(K \simeq 0)$, $\chi^{(3)}_{\max}$ and $\widetilde{\sigma}^{(2)}(\omega)$.

(ii) The giant oscillator strength model.—As discussed above, for the giant oscillator strength model one has to determine first the m wave function Ψ_m. Here, one can either use the biexciton wave function of Eq. (19) or the bipolariton wave function of Eq. (20).

(1) $\Psi_m = \Psi_0(p)$—the biexciton wave function of Eq. (19): This choice corresponds to the conventional interpretation of the giant oscillator strength model.[1–9]

The result of the numerical calculations of $\Gamma^m = \Gamma^m(K)$ with Eq. (62) is given in Fig. 9 (dashed line). Here, we again use the deuteron model wave function $\Psi_0(p)$ of Eq. (32) with $\epsilon^m_0 = 34$ meV. The calculated curve does not reproduce the experimental points for $K \to 0$, the corresponding $\Gamma^m(K = 0) = 160.0$ μeV. However, different model m wave functions $\Psi_0(p)$ can give the different values of $\Gamma^m(K = 0)$ even for the fixed m binding energy ϵ^m_0 (see, e.g., the discussions in Ref. 15).

The resonant value of $\chi^{(3)} = \chi^{(3)}(\omega = \Omega^{m(0)}_{\mathbf{p}+\mathbf{k}} - \omega_{\mathbf{k}}; \omega_{\mathbf{k}}, -\omega_{\mathbf{k}}, \Omega^{m(0)}_{\mathbf{p}+\mathbf{k}} - \omega_{\mathbf{k}})$ plays a crucial role in the unambiguous discrimination between the two models. According to Eq. (59),

$$\chi^{(3)}_{\max} = \chi^{(3)}(\omega = \Omega^{m(0)}_{\mathbf{p}+\mathbf{k}} - \omega_{\mathbf{k}}; \omega_{\mathbf{k}}, -\omega_{\mathbf{k}}, \Omega^{m(0)}_{\mathbf{p}+\mathbf{k}} - \omega_{\mathbf{k}}) \sim \frac{|\Psi_0\left(\frac{\mathbf{p}-\mathbf{k}}{2}\right)|^2}{\Gamma^m(\mathbf{p}+\mathbf{k})}\ , \tag{70}$$

where for the optical range one can put $|\Psi_0(\frac{\mathbf{p}-\mathbf{k}}{2})|^2 = |\Psi_0(0)|^2$. Thus, $\chi^{(3)}(\omega = \Omega^{m(0)}_{\mathbf{p}+\mathbf{k}} - \omega_{\mathbf{k}}; \omega_{\mathbf{k}}, -\omega_{\mathbf{k}}, \Omega^{m(0)}_{\mathbf{p}+\mathbf{k}} - \omega_{\mathbf{k}})$ is *insensitive* to Ψ_0 because for $K \ll a_m^{-1}$ the m radiative width $\Gamma^m(\mathbf{K} = \mathbf{p} + \mathbf{k})$ of Eq. (62) is also proportional to $|\Psi_0(p \simeq 0)|^2$ due to the δ function in the integrand. As a result, the wave function Ψ_0 *falls out* from the final expression of Eq. (70). From Eq. (59) one estimates $\chi^{(3)}(\omega = \Omega^{m(0)}_{\mathbf{p}+\mathbf{k}} - \omega_{\mathbf{k}}; \omega_{\mathbf{k}}, -\omega_{\mathbf{k}}, \Omega^{m(0)}_{\mathbf{p}+\mathbf{k}} - \omega_{\mathbf{k}}) = 0.18 \times 10^{-4}$ esu. This value, unique for the giant oscillator strength model, disagrees by one order of magnitude from our experimental data. The comparison of $\chi^{(3)}_{\max}$ and $\Gamma^m(K \simeq 0)$ of the two different models with the corresponding experimental values is summarized in Table I.

The calculated curves of the normalized integrated two-γ m absorption of the giant oscillator strength model without the interference terms[4,6–9,21] $\sim (\mathcal{E}_{\mathbf{k}}\mathcal{P}^*_{\mathbf{k}} + \mathrm{H.c.})$ are shown in Fig. 8 (dash-dotted line). This line shape does not reproduce the experimental points. However, the two-γ m absorption coefficient $K(\omega, \omega_{\mathbf{k}})$ of Eq. (60), which includes these interference terms of the giant os-

TABLE I. Comparison of optical properties.

	Bipolariton model	Giant oscillator strength model	Experimental results
Γ^m (μeV)	27.4	160.0	24 – 36
$\chi^{(3)}_{\max}$ ($\times10^{-4}$ esu)	1.05	0.18	1.7 – 3.0

cillator strength model, gives the integrated absorption $\widetilde{\sigma}^{(2)}(\omega)$ similar to the bipolariton model, if $|\omega_t - \omega_{\mathbf{k}})| \gg \Gamma^x$.

(2) $\Psi_m = \widetilde{\Psi}(\mathbf{p},\mathbf{k})/f(\mathbf{p},\mathbf{k})$—the bipolariton wave function of Eq. (20): In this way one automatically receives $\Gamma^m = \widetilde{\Gamma}^m$ from the bipolariton model. This value is in agreement with the experimental results.

However, the maximum resonant $\chi^{(3)} \geq 1$ esu evaluated by Eq. (59) with the bipolariton wave function of Eq. (27) considerably overestimates the corresponding experimental values. Formally, this result is due to the resonant bipolariton energy denominator $\delta\widetilde{\Omega}(\boldsymbol{l},\mathbf{K})$ of Eq. (27). In comparison with the exactly solvable bipolariton model, the giant oscillator strength model cannot remove this feature from $\chi^{(3)}$ and $K^{(2)}$ of Eqs. (59) and (60) [see also Eq. (61)].

The integrated absorption coefficient $\widetilde{\sigma}^{(2)}(\omega)$ calculated with Eq. (61) is shown in Fig. 8 (dashed line). The corresponding curves fit the experimental points worse than the bipolariton model. However, the main qualitative shortcoming of the giant oscillator strength model with the bipolariton wave function $\Psi_m = \widetilde{\Psi}/f$ is a non-Lorentzian absorption line of Eq. (61).

V. CONCLUSIONS

In this work we have developed and applied the concept of a bipolariton in order to analyze the nonlinear optical response of an m state. This concept treats an m as a metastable state of the two polaritons quasibound through the Coulombic interaction of their x components. Then, the m optical decay and the two-γ m optical generation are mutually inverse processes in terms of resonant polariton-polariton scattering.

The main conclusions of the work are as follows.

(i) The exactly solvable bipolariton model is worked out for the deuteron potential of the x-x interaction. This model allows us to calculate self-consistently within the x-γ dynamical system all the m optical characteristics: the m radiative width $\widetilde{\Gamma}^m$ and the radiative correction Δ^m (the m Lamb shift) of the m energy Ω^m, the third-order m nonlinear susceptibility $\chi^{(3)}$, and the two-γ m absorption coefficient $K^{(2)}$.

(ii) The high-precision measurements in CuCl of Γ^m, $\chi^{(3)}$, and $K^{(2)}$ discriminate the bipolariton and giant oscillator strength models in favor of the first one.

ACKNOWLEDGMENTS

We appreciate valuable discussions with L.V. Keldysh, Y. Toyozawa, and K. Cho. We acknowledge the technical assistance of H. Kawano and M. Nishino. This work has been supported by the Grant-in-Aid for General Scientific Research from the Ministry of Education, Science and Culture, Japan and by the Volkswagen Stiftung, Germany.

[1] M. Ueta, H. Kanzaki, K. Kobayashi, Y. Toyozawa, and E. Hanamura, *Excitonic Processes in Solids*, Springer Series in Solid State Sciences Vol. 60 (Springer, Berlin, 1986), Chaps. 2 and 3.

[2] E. Hanamura and H. Haug, Phys. Rep. **33**, 209 (1977); C. Klingshirn and H. Haug, *ibid.* **70**, 315 (1981).

[3] A.A. Gogolin and E.I. Rashba, Pis'ma Zh. Eksp. Teor. Fiz. **17**, 690 (1973) [JETP Lett. **17**, 478 (1973)].

[4] E. Hanamura, Solid State Commun. **12**, 951 (1973).

[5] F. Henneberger and J. Voigt, Phys. Status Solidi B **76**, 313 (1976); V. May, K. Henneberger, and F. Henneberger, *ibid.* **94**, 611 (1979); F. Henneberger and V. May, *ibid.* **109**, K139 (1982).

[6] P.I. Khadzhi, S.A. Moskalenko, and S.N. Belkin, Pis'ma Zh. Eksp. Teor. Fiz. **29**, 223 (1979) [JETP Lett. **29**, 200 (1979)].

[7] H. Haug, R. März, and S. Schmitt-Rink, Phys. Lett. **77A**, 287 (1980); S. Schmitt-Rink and H. Haug, Phys. Status Solidi B **108**, 377 (1981); S.W. Koch and H. Haug, Phys. Rev. Lett. **46**, 450 (1981); S. Schmitt-Rink and H. Haug, Phys. Status Solidi B **113**, K143 (1982); H. Haug, in *Festkörperprobleme (Advances in Solid State Physics)*, edited by J. Treusch (Vieweg, Braunschweig, 1982), Vol. XXII, p. 149.

[8] I. Abram, Phys. Rev. B **28**, 4433 (1983).

[9] K. Cho, J. Phys. Soc. Jpn. **54**, 4444 (1985).

[10] G.M. Gale and A. Mysyrowicz, Phys. Rev. Lett. **32**, 727 (1974).

[11] N. Nagasawa, N. Nakata, Y. Doi, and M. Ueta, J. Phys. Soc. Jpn. **39**, 987 (1975); V.D. Phach, A. Bivas, B. Hönerlage, and J.B. Grun, Phys. Status Solidi B **84**, 731 (1977).

[12] N. Nagasawa, S. Koizumi, T. Mita, and M. Ueta, J. Lumin. **12-13**, 587 (1976); N. Nagasawa, T. Mita, and M. Ueta, J. Phys. Soc. Jpn. **41**, 929 (1976); B. Hönerlage, A. Bivas, and V.D. Phach, Phys. Rev. Lett. **41**, 49 (1978).

[13] D.S. Chemla, A. Maruani, and E. Batifol, Phys. Rev. Lett. **42**, 1075 (1979); A. Maruani and D.S. Chemla, Phys. Rev. B **23**, 841 (1981).

[14] N. Nagasawa, M. Kuwata, E. Hanamura, T. Itoh, and A. Mysyrowicz, Appl. Phys. Lett. **55**, 1999 (1989).

[15] H. Akiyama, M. Kuwata, T. Kuga, and M. Matsuoka, Phys. Rev. B **39**, 12 973 (1989); H. Akiyama, T. Kuga, M. Matsuoka, and M. Kuwata-Gonokami, *ibid.* **42**, 5621 (1990).

[16] R. Shimano and M. Kuwata-Gonokami, Phys. Rev. Lett. **72**, 530 (1994).

[17] T. Ikehara and T. Itoh, Solid State Commun. **79**, 755 (1991).

[18] M. Hasuo, N. Nagasawa, and T. Itoh, Opt. Commun. **85**, 219 (1991); M. Hasuo, M. Nishino, and N. Nagasawa, J. Lumin. **60-61**, 672 (1994).

[19] J.J. Hopfield, Phys. Rev. **182**, 945 (1968).

[20] L.D. Landau and E.M. Lifshitz, *Course of Theoretical Physics* (Pergamon, Oxford, 1965), Vol. 3, Chap. 17.

[21] A.L. Ivanov and H. Haug, Phys. Rev. B **48**, 1490 (1993).

[22] A.L. Ivanov and H. Haug, Phys. Rev. Lett. **74**, 438 (1995); Phys. Status Solidi B **188**, 61 (1995).
[23] M. Ojima, T. Kushida, Y. Tanaka, and S. Shionoya, J. Phys. Soc. Jpn. **44**, 1294 (1978).
[24] M.I. Sheboul and W. Ekardt, Phys. Status Solidi B **73**, 165 (1976); H. Haug and S. Schmitt-Rink, Prog. Quantum Electron. **9**, 3 (1984).
[25] L.V. Keldysh, in *Bose-Einstein Condensation*, edited by A. Griffin, D.W. Snoke, and S. Stringari (Cambridge, New York, 1995), p. 246.
[26] E.M. Lifshitz and L.P. Pitaivskii, *Course of Theoretical Physics* (Pergamon, Oxford, 1983), Vol. 9, Part II, Secs. 16 and 31.
[27] P. Nozieres, *Theory of Interacting Fermi System* (Benjamin, New York, 1964), Sec. 6.2.
[28] O. Akimoto and E. Hanamura, J. Phys. Soc. Jpn. **33**, 1537 (1972); W.F. Brinkman, T.M. Rice, and B. Bell, Phys. Rev. B **8**, 1570 (1973).
[29] V. May and J. Röseler, Phys. Status Solidi B **102**, 533 (1980).
[30] A.L. Ivanov and V.V. Panashchenko, Zh. Eksp. Teor. Fiz. **99**, 1579 (1991) [Sov. Phys. JETP **72**, 882 (1991)].
[31] Y.R. Shen, *The Principles of Nonlinear Optics* (John Wiley, New York, 1984), p. 203.
[32] M. Hasuo, H. Kawano, and N. Nagasawa, Phys. Status Solidi B **188**, 77 (1995).